Emergence of Jupiter's vortices and jets from random initial conditions

F. BOUCHET[1,2] and T. DUMONT[3]

[1]Institut Fourier, UMR 5582, Grenoble France
[2]Dipartimento di Energetica "Sergio Stecco", Università degli studi di Firenze, Italy
[2]Laboratoire d'Analyse Numérique-CNRS UMR 5585 Université Lyon 1 France

2nd February 2008

Received:
Author version:
Author contact : bouchet@dma.unifi.it

Abstract

We explain the emergence and stability of the most important jets and vortices, in the highly turbulent Jupiter's atmosphere, by a statistical mechanics of the potential vorticity mixing. Using the Quasi-Geostrophic 1-1/2 layer, with topography, when the Rossby deformation radius is small, we predict strong jets. These jets can be either zonal, or closed into a ring structure like the Great Red Spot one. We reproduce the GRS observed velocity field to a very good quantitative accuracy. For smaller vortices, or for stronger topography curvature, we reproduce the characteristics properties of the White Ovals or of the cyclonic Brown Barges. The link between their shape, topography and surrounding shear is explicitly described. We obtain very strong qualitative results for the Jupiter's vortices. For instance, any of these vortices must be on topography extrema (in the reference frame moving with the structure), the shear in the active layer is larger than the shear in the deep layer. On a same latitudinal band, the velocity of the vortex is related to their latitude. These theoretical predictions are in accordance with the observed properties of Jovian vortices.

1 Introduction

Atmospheric and oceanic flows have the property to organize into large scale jets or vortices. Due to the large difference between typical forcing and inertial time scales, this organization is remarkably stationary in the case of Jupiter's troposphere. The understanding of the stability and of the detailed structure of these flows is thus render easier than for any other geophysical flows. Moreover, the excellent quality of the data obtained from space probes, makes easy a precise comparison of theoretical predictions with actual flows.

As in the oceans and in the earth atmosphere, these flows are often organized into narrow jets. They can zonally flow around the planet, like the eastward jet at 24^0 latitude in the northern hemisphere of Jupiter (Maxworthy 1984), or alternatively organize into rings, forming vortices, like the rings shed by the meandering of the Gulf-Stream in the western Atlantic Ocean. The flow field in Jupiter most famous feature, the Great Red Spot, is an oval-shaped jet, rotating in the anticyclonic direction and surrounding an interior area with a weak mean flow (Dowling and Ingersoll 1989) (see figure 1). Robust cyclonic vortices are also observed with a similar jet structure (Hatzes et al 1981), see figure 13. Smaller features, as the White Ovals, have also an oval shape but without the jet ring structure. For a recent review on the dynamics of Jupiter's atmosphere, see Ingersoll and collaborators (2003).

A number of numerical studies have been led to model the Jupiter's vortices (see Ingersoll and collaborators 2003, for a review). The Kida vortex (Kida 1981) has been used to explain the typical oval shape of such vortices (Polvani and collaborators 1990). Some soliton like structures have been also describe (Petviashvili 1981, ????) with similar shapes. Anyway, none of these analytical and theoretical models, reproduce both the oval shape and ring structure of the Great Red Spot. We will argue that the strong jets are the consequence of a small value of the Rossby deformation radius, for very energetic flows. With such parameters, the effect of a topography (deep flow and beta effect) will be necessary to explain the typical oval shape. Moreover, such jets and vortices are in a turbulent surrounding, and the persistence of their strength and concentration in the presence of eddy mixing is intriguing and should be explained.

The explanation proposed in this paper is based on a statistical mechanical approach: the narrow jet or vortex appears as the most probable state of the flow after a turbulent mixing of potential vorticity, taking into account constraints due to the dynamical conserved quantities, especially energy. Such a statistical theory has been first proposed for the two-dimensional incompressible Euler equations by Kuz'min (1982), Robert (1990), Robert and Sommeria (1991), Miller (1990), see Sommeria (2001) for a recent review. This theory predicts an organization of 2D turbulence into a steady flow, superposed with fine scale, 'microscopic' vorticity fluctuations. This is by far the most likely result of random stirring, so the evolution to this statistical equilibrium is in practice irreversible. Complete vorticity mixing is prevented by the conservation of the energy, which can be expressed as a constraint in the accessible vorticity fields. A similar, but quantitatively different, organization had been previously obtained with statistical mechanics of singular point vortices, instead of continuous vorticity fields (Onsager 1949, Joyce and Montgomery 1973). The possibility of using such ideas to explain the Great Red Spot has been explicitly quoted since the first works on the 2D Euler statistical mechanics by Robert (1990), Miller (1990), Sommeria et al (1991), Miller Weichman and Cross (1992), Turkington, Majda and DiBattista (2001), but without explicit predictions.

In the study of geophysical flows, the Rossby deformation radius is a central parameter, as it defines a typical scale for the variation of the pressure. In a previous paper (Bouchet and Sommeria, 2002), we have analytically described the statistical equilibrium states, for the Quasi-Geostrophic equation, in the limit of a small Rossby deformation radius. In this limit, the equilibrium flows are characterized by strong jets, either zonal and flowing around the planet or forming closed vortices, depending on the parameters. When a topography is considered, these vortices have the typical shape of Jovian ones'. We have also shown that these equilibrium are able to reproduce quantitatively all the main characteristics of the Great Red Spot. In section 2.3, we will give a simplified derivation of these results. Whereas in Bouchet and Sommeria 2002, the statistical equilibrium were analyzed for the simple case of a potential vorticity distribution made of two levels, we extensively discuss the generalization of the results to any PV distribution. We show that the main results do not depend on the detailed distribution. This is true as a consequence of the small value of the Rossby deformation radius.

In section 2.4, we discuss the application of such results to the Jovian vortices. We discuss a simple model for the Great Red Spot, also present in Bouchet and Sommeria (2002). We discuss important qualitative predictions for such vortices : they are located on extrema of the topography, their energy must be greater than a critical one, the shear on the active layer has to be stronger than in the deep layer, their typical width is given by an alternative of the Rhine's scale, which no does not depends on the beta-effect, but on the topography curvature.

The limit of small Rossby radius is no more valid for smaller vortices, such as the Brown Barges or the White Ovals. In order to model these features, we will numerically compute the velocity fields of the statistical equilibrium states. Using the qualitative comprehension obtained from the analytical analysis, we will be able to reproduce the main properties of these flows, either from the destabilization of jets, or from random Potential Vorticity initial conditions. In section 3 we obtain a velocity field close to the White-Oval one. In section 4, we obtain numerically the velocity field of the Great Red Spot which is accurately

compared to the observed one's. In section 6, we obtain the peculiar velocity field of the Brown Barges, with a jet like structure in the meridional direction, and a strong shear in the zonal one.

In section 5, we comment results of Ellis, Haven and Turkington (2002), on the stability of statistical equilibrium. We illustrate the corresponding results by numerical experiment of stabilization or destabilization of strong jets. This complete the explanation of the emergence and of the stability of Jupiter's features in the Jupiter's turbulent atmosphere.

2 Statistical mechanics of the Quasi-Geostrophic equation in the limit of small Rossby deformation radius

In this section we present the Quasi-Geostrophic 1-1/2 layer model and the main ideas of the potential vorticity statistical mechanics. This theory describes the most probable state, emerging from a random PV field with a given PV distribution and energy. The main hypothesis is that these equilibrium structures emerge from the very complex dynamical mixing. These stationary states have been described analytically in a previous work (Bouchet and Sommeria 2002), for the Quasi-Geostrophic model, in the limit of small Rossby deformation radius. In this section we sketch the main ideas of this derivation and the main results and consequence in the context of the Jovian troposphere. These results explain in particular the formation of jets or vortices from random initial conditions. Such vortices have the annular jet structure characteristic of the Great Red Spot and their main characteristics are analytically related.

In the following sections we will propose numerical simulation, illustrating these main results, and permitting to compare them to the main structures of the Jovian troposphere : the strong jets, the north hemisphere Brown Barges, the White Ovals, and the Great Red Spot.

2.1 The dynamical system

We start from the barotropic 1-1/2 Quasi Geostrophic (QG) equation :

$$\frac{\partial q}{\partial t} + \mathbf{v} \cdot \nabla q = 0 \tag{1}$$

$$q = -\Delta\psi + \frac{\psi}{R^2} - Rh(y) \tag{2}$$

$$\mathbf{v} = -\mathbf{e}_z \wedge \nabla\psi \tag{3}$$

where q is the potential vorticity (PV), advected by the non-divergent velocity $\mathbf{v}$, ψ is the stream function[1], R is the internal Rossby deformation radius between the layer of fluid

[1]We choose for the stream function ψ the standard sign convention used for the Euler equation, which is just the opposite as the one commonly used in geophysical fluid dynamics. Our stream function ψ is therefore proportional to the opposite of the pressure fluctuation in the northern hemisphere and to the pressure fluctuation in the southern hemisphere, as the planetary vorticity sign is reversed. The signs of q and $\mathbf{v}$ are not influenced by this choice of sign for ψ.

under consideration and a deep thicker layer, unaffected by the dynamics. x and y are respectively the zonal and meridional coordinates (x is directed eastward and y northward).

The term $Rh(y)$ represents the combined effect of the planetary vorticity gradient and of a given stationary zonal flow in the deep layer, with stream function $\psi_d(y)$: $Rh(y) = -\beta y + \psi_d/R^2$. This deep flow induces a constant deformation of the free surface, acting like a topography on the active layer[2]. We shall therefore call $h(y)$ the 'topography'. We scale the topography with the Rossby deformation radius R. This particular choice will be of importance in the study of the limit $R \to 0$ (section 2.3) and we will show that this scaling is the appropriate one to study Jovian vortices.

We define the QG equations (1,2) with periodic boundary conditions (4π periodic in the zonal direction and π periodic in the meridional one for all numerical computations of this article). The analytical study in Bouchet and Sommeria 2002 has shown that, in the channel geometry, due to the small value of the Rossby deformation radius, the equilibrium organization of the flow is local. For instance vortices are located on topography extrema and their structure and shape is determined by the topography curvature and is independent on boundary conditions. In the periodic boundary conditions case, we will show in the following that this is still true. This local organization explains why periodic boundary condition is well suited to vortices structure studies. On the contrary, the global organization of zones and bands on the planet scale should be tackled using a real spherical geometry, for instance in the Shallow Water model. This more general problem will not be considered in this article.

We model one zone and band area by a periodic topography:

$$h(y) = -2a\cos(2y) \tag{4}$$

As the relevant scale is defined by the latitudinal variations of the topography, we do not respect the actual zonal band aspect ratio, and we scale the domain size on the latitudinal zone-band extension. In our dimensionless variable $R = \pi R^\star/L^\star$ where $R^\star$ is the actual internal Rossby deformation radius and $L^\star$ is the latitudinal extension of the zone-band domain.

Let $\langle f\rangle \equiv \int_D f d^2\mathbf{r}$ be the average of f on D for any function f. Physically, as the stream function ψ is related to the geostrophic pressure, $\langle\psi\rangle$ is proportional to the mean height at the interface between the fluid layer and the bottom layer, and due to the mass conservation it must be constant (Pedlosky 1987). We make the choices $\langle\psi\rangle = 0$ and $\langle h\rangle = 0$ without loss of generality. The total circulation is $\langle q\rangle = \langle -\Delta\psi + \psi/R^2 - Rh(y)\rangle$ is equal $\langle\psi/R^2\rangle$ due to the periodic boundary conditions. Therefore $\langle q\rangle = 0$.

Due to the periodic conditions for ψ, the linear momentum is also equal to 0,

$$\langle\mathbf{v}\rangle = 0 \tag{5}$$

[2]A real topography $\eta(y)$ would correspond to $Rh(y) = -f_0\eta(y)/h_0$ where f_0 is the reference planetary vorticity at the latitude under consideration and h_0 is the mean upper layer thickness. Due to the sign of f_0, the signs of h and η would be the same in the south hemisphere and opposite in the north hemisphere. As we will discuss extensively the Jovian south hemisphere vortices, we have chosen this sign convention for h.

The energy

$$E = \frac{1}{2}\int_D (q + Rh)\,\psi d^2\mathbf{r} = \frac{1}{2}\int_D \left[(\nabla\psi)^2 + \frac{\psi^2}{R^2}\right] d^2\mathbf{r} \tag{6}$$

is conserved (we note that the first term in the right hand side of (6) is the kinetic energy whereas the second one is the gravitational available potential energy).

The Casimir integrals

$$C_f(q) = \int_D f(q) d^2\mathbf{r} \tag{7}$$

for any continuous function f, in particular the different moments of the PV, are also conserved.

2.2 The statistical mechanics on a two PV levels configuration.

2.2.1 The macroscopic description.

The QG equations (1) (2) are known to develop very complex vorticity filaments. Because of the rapidly increasing amount of information it would require, a deterministic description of the flow for long time is both unrealistic and meaningless. The statistical theory adopts a probabilistic description for the vorticity field. We consider the local probability to have some PV at some points. The statistical equilibrium is then the most probable state for a random PV field with fixed dynamical invariants.

The statistical equilibrium therefore depends on the energy (6) and on the infinite number of Casimirs (7) (PV distribution). For pedagogical reasons, we will consider the most simple case we will suppose a distribution made of two PV levels, denoted $q = a_1$ and $q = a_{-1}$. The results may however be generalized (Robert and Sommeria 1992). In section 2.3, we will explain why the study of the equilibrium structures is independent of the actual PV distribution, at the lower order when the Rossby radius goes to zero.

The two values of the PV $q = a_1$ and $q = a_{-1}$, and the areas A and $(1 - A)$ they respectively occupy in D, will be conserved by the inertial dynamics (this is then equivalent to the conservation of all the Casimirs (7)). The determination of the statistical equilibrium then depends only on the energy E, on the two PV levels a_1 and a_{-1} and on the area A. The number of free parameters can be further reduced by appropriate scaling. Indeed a change in the time unit permits to define the PV levels up to a multiplicative constant. We choose for the sake of simplicity :

$$\frac{a_1 - a_{-1}}{2} = 1 \tag{8}$$

and define the non-dimensional parameter B as :

$$B \equiv \frac{a_1 + a_{-1}}{2} \tag{9}$$

As discussed previously the mean PV is equal to zero, this imposes that $a_1 A + a_{-1}(1-A) = 0$. This means that a_1 and a_{-1} must be of opposite sign and, using (8) and (9), $A = (1-B)/2$. The distribution of PV levels is therefore fully characterized by the single asymmetry parameter B, which takes values between -1 and +1. The symmetric case of two PV patches

with equal area $A = 1/2$ corresponds to $B = 0$, while the case of a patch with small area (but high PV, such that $\langle q \rangle = 0$) corresponds to $B \to 1$. Note that we can restrict the discussion to $B \geq 1$ as the QG system is symmetric by a change of sign of the PV.

The two PV levels mix due to turbulent dynamics, and the resulting state is locally described by the local probability (local area proportion) $p(\mathbf{r})$ to find the first level at the location $\mathbf{r}$. The probability to find the complementary PV level a_{-1} is $1-p$, and the locally averaged PV at each point is then

$$\overline{q}(\mathbf{r}) = a_1 p(\mathbf{r}) + a_{-1}(1 - p(\mathbf{r})) = 2\left(p - \frac{1}{2}\right) + B \tag{10}$$

where the second relation is obtained by using (8) and (9).

Since the patch with PV level a_1 is mixed but globally conserved, the integral of its density p over the domain must be equal to the initial area A,

$$A \equiv \frac{1-B}{2} = \int_D p(\mathbf{r}) d^2\mathbf{r} \tag{11}$$

We note that the inertial conservation of the Casimir, is taken into account in the microscopic description, by the knowledge of the distribution of the PV. However the coarse-graining (macroscopic description) does not preserves the value of the Casimirs (7): $C_f(q) \neq C_f(\overline{q})$, except for the first moment.

The effect of local PV fluctuations on the stream function is filtered out by integration of equation 2 ($\overline{\psi} = \psi$ and $\overline{\mathbf{v}} = \mathbf{v}$), the stream function and the velocity field are thus fully determined by the locally averaged PV $\overline{q}$ as the solution of

$$\overline{q} = -\Delta\psi + \frac{\psi}{R^2} - Rh(y) \ ; \ \psi \ \ periodic \tag{12}$$

$$and \quad \mathbf{v} = -\mathbf{e}_z \wedge \nabla\psi$$

Therefore the energy is also expressed in terms of the field $\overline{q}$:

$$E = \frac{1}{2}\int_D \left[\ (\nabla\psi)^2 + \frac{\psi^2}{R^2} \ \right] d^2\mathbf{r} = \frac{1}{2}\int_D (q + Rh)\,\psi d^2\mathbf{r} \tag{13}$$

From now on we forget the q over-line for the locally averaged PV and refer to it as the PV.

The central result of the statistical mechanics of the QG equations (1,2) is that the most probable mixing of the potential vorticity is given by the maximization of the entropy

$$S = -\int_D [\ p(\mathbf{r}) \ln p(\mathbf{r}) + (1 - p(\mathbf{r})) \ln(1 - p(\mathbf{r}))\ ] d^2\mathbf{r} \tag{14}$$

under the constraints of the global PV distribution (11) and energy (13). It can be shown that the microscopic states satisfying the constraints given by the conservation laws are overwhelmingly concentrated near the Gibbs state. A good justification of this statement is obtained by the construction of converging sequences of approximations of the QG equation

(1,2), in finite dimensional vector spaces, for which a Liouville theorem holds. This is a straightforward translation of the work of Robert (1999) for 2D Euler equations. The sequence of such Liouville measures has then the desired concentration properties as (1,2) enters in the context considered in Michel & Robert (1994 b). More recently; Ellis (1999) also discussed such large deviation results together with other systems.

Once the most probable state is found, we suppose that it describes observed flows. The ergodicity of the system would be sufficient to justify this. But, as in usual statistical mechanics (for instance for gas) this ergodic property of a system is very unlikely to be proven for any generic system and could moreover appear to be wrong in general. A weaker property of mixing is however sufficient to justify statistical mechanics due to the concentration property stated in the above paragraph. The Gibbs state is most likely to be reached even if the available microscopic states are not evenly explored. In practice, the theory can be validated or invalidated only on the basis of its success or failure to predict well characterized phenomena.

2.2.2 The Gibbs states

We want to describe the equilibrium structures (Gibbs states). We thus seek the maxima of the entropy (14) under the constraints of the area (11) and energy (13):

$$\max \{S \,|\, \text{with } E = E_0 \text{ and } A = (1-B)/2\} \tag{15}$$

In Bouchet and Sommeria (2002), we have studied this variational problem in the limit of small Rossby deformation radius. The study of such a variational problem is rendered difficult by the two constraints. In the following, we will argue that for the present case, this technical difficulty may be circumvented. We will then proposed a more straightforward derivation of Bouchet and Sommeria (2002) results. The main ideas are however the same. For this, let us consider the following variational problem:

$$\left\{ \begin{array}{c} \min \{\mathcal{F}[\phi] \,|\, \text{with } A[\phi] = -\alpha\} \\ \text{with } \mathcal{F} = \int_D d\mathbf{r} \left[\frac{R^2(\nabla\phi)^2}{2} + f_C(\phi) - R\phi h(y) \right] \;,\; \mathcal{A}[\phi] = \int_D d\mathbf{r}\, \phi \\ \text{and } f_C(\phi) = \phi^2/2 - \ln(\cosh(C\phi))/C \end{array} \right. \tag{16}$$

We will call $\mathcal{F}$ the modified free energy. This variational problem (16) involves only one variable ϕ whereas the entropy maximization involves the two variables p (or q) and ψ. Moreover, the energy constraint has been absorbed. It is thus simpler than the maximization of the entropy with two constraints. Moreover, as we shall see in section 2.3, the peculiar shape of the function f_C, with two minima (see figure 2) will allow us to have a direct hint on the structure of the solution.

Let us compute the equation verified by the critical states (the Euler-Lagrange equations) of the modified free energy (16). For this we consider small variations $\delta\phi$ of the functional $\mathcal{F} + R\alpha_1\mathcal{A}$, where $-R\alpha_1$ is the Lagrange parameter associated to the conservation of the area $\mathcal{A}$. After straightforward computations, we obtain:

$$-R^2\Delta\phi + \phi - Rh(y) = \tanh(C\phi) - R\alpha_1 \tag{17}$$

Let us suppose that ϕ minimize this variational problem. Let us then define the stream function ψ by:

$$\psi = R^2 (\phi + \alpha) \tag{18}$$

If we use the relation (18), setting $\alpha - R\alpha_1 = B$, we obtain the following equation: $q = -\Delta\psi + \psi/R^2 - Rh(y) = B + \tanh\left(C\left(\psi/R^2 - \alpha\right)\right)$. This equation is also the critical point of maximization of the entropy (15) (see Bouchet and Sommeria 2002), where $C\alpha$ and $\beta = -C/R^2$ are the Lagrange parameters associated to the conservation of the area and of the energy respectively. This equation describes a stationary solution of the Quasi-Geostrophic equation. These two equations, for the stream function ψ, or for ϕ (17) will be called the Gibbs state equations.
We have shown that the critical points of the modified free energy (16) are also critical point of the maximization of the entropy under constraint (15). However, this does not prove that the *minima* of the free energy are actually *maxima* of the entropy under the constraints. It can be proven on a very general ground (see Bouchet and Barré 2003) that any minimum of the free energy $F = S/\beta - E$, with the area constraint, is a minima of the entropy with energy and area constraint (15) (the converse in wrong in general). We can thus study the minimization of the free energy, and verify afterwards that all the possible energy are obtained. This will be the case in our study, in the limit of small Rossby deformation radius. To prove that the minimization, with area constraint, of the free energy and of the modified free energy (16) are equivalent, one can either explicitly study the stability of the solutions or prove that these two variational problem are equivalent to a third one with two independent variables ψ and ϕ. This point is addressed in in Bouchet (2001), proving that minima of the modified free energy are maxima of the entropy with constraints.

2.3 The limit of small Rossby deformation radius.

In this section, we analyze the solution of the minimization of the modified free energy $\mathcal{F}$ (16) with the constraint of the area $\mathcal{A}$, in the limit of small deformation radius. We will always consider $C > 1$.

We have to minimize the functional $\mathcal{F} = \int_D d\mathbf{r} \left[\frac{R^2(\nabla\phi)^2}{2} + f_C(\phi) - R\phi h(y)\right]$ with a constraint. The modified free energy reduces, at lower oder in R, to the minimization of $\int_D d\mathbf{r}\, f_C(\phi)$. The actual shape of the function f_C will therefore be essential to the discussion. Figure 2 shows this shape when $C > 1$ (see 16 for the definition of f_C). This figure shows that f_C is even and possess two minima that we shall denote $\pm u$. u verify:

$$u = \tanh(Cu). \tag{19}$$

The minimization of this functional, without the topography term, also represents the coexistence of two phases in a situation of first order phase transitions in classical thermodynamics (Van-Der-Walls Cahn-Hilliard model). Let us discuss it, for instance, for a coexistence between a gas and a liquid phases. The two minimum value of the volume free energy f_C then correspond to the specific volume of each phase at equilibrium. The constraint then fixes the respective volume occupied by the two phases. When first order terms are considered, the gradient term describes the transition surface between one phase to the other. A

surface free energy is then associated to this transition. The minimization of this surface free energy then leads to bubble for equilibrium structures.

We note that the mathematical study of functional of the type 16, but without the topography, is considered in Modica (1987). The functional analysis study of this work, prove the hypothesis at the base of this qualitative description: ϕ will take the two values $\pm u$ in subdomains separated by transition area of width scaling with R. Using this, we will propose a very intuitive asymptotic expansion to describe the solutions (please note that our problem is two-dimensional, surfaces will be replaced by lines). With respect to Modica work, our expansion will allows a precise description of the jet, and the generalization of the results when a topography term is taken into account. A more complete and satisfying description of the whole asymptotic expansion, generalizable at all order in R, with mathematical justification of the existence of the solutions for the jet equation at all order in R, is provided in Bouchet (2001). Higher order effects are also discussed in this work. We now present a simplified discussion.

For vortices, the two phases correspond to two different value of the mixing of the PV. The conservation of the volume corresponds to the conservation of the global PV. As we will see, the effect of the topography will lead to a balance between the minimization of the length free energy and of the tendency of positive PV to stand around extrema of the topography, leading to the very characteristic elongated shape of Jovian vortices.

2.3.1 The zeroth order stream function outside of the jet: a quiescent core

At lower order the value of ϕ will therefore take the two values u and $-u$ in two subdomains, denoted respectively A_+ and A_-, as illustrated in figure (3). The constraint $\mathcal{A}[\phi] = \int_D d\mathbf{r}\, \phi = -\alpha$, taking $A_+ + A_- = 1$, will determine the respective area occupied by these two values: $2A_\pm = (1 \mp \alpha/u)$. This implies $u > \alpha$. The actual subdomain shape will be determined by the second order analysis. At this stage the two domains A_+ or A_- may also not be connected.

The above discussion solve the first order problem. Using the link between ϕ and the stream function (18), we can compute the first order values of ψ: $\psi_\pm = R^2(\pm u + \alpha)$, the corresponding value of B: $B = -\int_D d\mathbf{r}\, (\tanh(C\phi)) = uA_- - uA_+ = \alpha$, and the corresponding value of the energy (13) : $2R^2E = \psi_+^2 A_+ + \psi_-^2 A_-$. This yields $2E = R^2\left(u^2 - \alpha^2\right)$, where u is a function of C given by (19).

For sake of simplicity, we parameterize the state by the two parameters u and B, with $u > B$. We thus obtain, at lower order in R :

$$\psi_\pm = R^2(B \pm u) \tag{20}$$

$$A_\pm = \frac{1}{2}\left(1 \mp \frac{B}{u}\right) \tag{21}$$

and

$$E \simeq E_A = \frac{R^2}{2}(u^2 - B^2) + \mathcal{O}(R) \tag{22}$$

Therefore all the quantities are determined from the asymmetry parameter B and from the parameter u, related to the energy by (22).

In the limit of low energy, $u \to |B|$, when for instance $B > 0$, then A_1 goes to zero, so that ψ_{-1} tends to occupy the whole domain. This state is the most mixed one compatible with the constraint of a given value of B (or equivalently a given initial patch area $A = (1-B)/2$). In the opposite limit $u \to 1$, we see from (20) that in the two subdomains $q = \psi/R^2$ tends to the two initial PV levels $a_1 = 1 + B$ and $a_{-1} = -1 + B$. Thus, this state is an unmixed state. It achieves the maximum possible energy $E = \frac{R^2}{2}(1 - B^2)$ under the constraint of a given patch area. We conclude that the parameter u, or the related 'temperature' C_0, characterizes the mixing of these two PV levels. We shall call u the segregation parameter, as it quantifies the segregation of the PV level a_1 (or its complementary a_{-1}) between the two phases.

2.3.2 The strong jet equation

As stated before, the preceding analysis does not take into account the interface between the two area $A_\pm$. At this interface, the value of ϕ, and thus of the stream function will change rapidly, on a scale of order R. It will thus corresponds to a strong jet. To analyze this interface, we consider the Gibbs states equation (17) at the lower order in R. Using that the interface develops on a length scale of order R, we consider τ the coordinate normal to the jet, rescaled by R: $\zeta = R\tau$. In the Laplacian term, we neglect the curvature which has to be taken into account at the first order in R. We then obtain:

$$-\frac{d^2\phi}{d\zeta^2} = \tanh(C\phi) - \phi = -\frac{d}{d\phi} f_C(\phi) \tag{23}$$

The jet equation is thus the equation of a particle position ϕ in a potential $-f_C(\phi)$. As $f_C(\phi)$ has exactly two minima: $f(\pm u)$, there is a unique trajectory with limit conditions $\phi \to \pm u$ for $\zeta \to \pm\infty$.

This analysis shows that the jet scales typically as the Rossby deformation radius. Moreover, in dimensionless units, the jet width and the jet maximum velocity are given by $Rl(u)$ and $Rv_{max}(u)$ where l and v_{max} are functions of u that may be numerically tabulated from the resolution of the previous differential equation. These relations allow to compute u from the jet properties.

2.3.3 The first order stream function outside of the jet: the weak shear flow

To determine the first order stream function outside of the jet, we consider the Gibbs state equation (17) by neglecting the Laplacian term. We thus obtain the algebraic equation: $\phi - Rh(y) = \tanh(C\phi) - R\alpha_1$. Using that $\phi = \pm u$ at zero order, we calculate the first order solution to this equation. Using the results (19), this yields $\phi = \pm u + R\delta\phi = \pm u + R\left(h(y) + \alpha_1\right) / \left(1 - C(1-u^2)\right)$. Using the link between ϕ and the stream function (18) and the link between the stream function and the velocity (3), we obtain:

$$\mathbf{v} = R^3 \left(\frac{dh/dy}{1 - C(1-u^2)} \right) \mathbf{e}_x \tag{24}$$

This relates the zonal flow outside of the jets, the topography, and the parameter u (determined from the total energy or from the jet properties).

2.3.4 Determination of the vortex shape: the typical elongated shape

Until now the jet shape has not been determined. To determine it we can alternatively consider the jet equation at first order or compute the first order modified free energy $\mathcal{F}$ (16). We make this second choice as it will enlightened the interpretation of the solution.

The zero order modified free energy $\mathcal{F}_0$ could be computed from the value of $\phi = \pm u$ outside of the jet and from the areas $A_\pm$ (21). As it is not of interest for the following discussion, we don't do it explicitly. Let us call $R\delta\phi$ the first order modification of ϕ, computed in the previous section. It gives the contribution $R\int_D d\mathbf{r}\, df_C(\pm u)\delta\phi$ to the modified free energy, at first order. But as by definition of u, $df_C(\pm u) = 0$, this contribution is null. Let us compute the first order contribution of the topography term $RH = \int_D d\mathbf{r}\ (-R\phi h(y))$. For this we use the zero order result $\phi = \pm u$. We then obtain $H = H_0 - 2u\int_{A_+} d\mathbf{r}\, h(y)$, where $H_0 \equiv u\int_D d\mathbf{r}\, h(y)$. We note that H_0 does not depends on the jet shape. The last contribution comes from the jet. As the jet scales like R, to determine the jet contribution at first order in R, we only need the jet determination at zeroth order. It is then easy to convince oneself that the jet contribution is proportional to its length L: it will have the form $Re\,(u)\,L$ where $e(u)$ depends only on the zeroth order jet property, itself described by (23). One can then obtain $2e\,(u) = \int_{-\infty}^{+\infty}\left(\frac{d\phi}{d\tau}\right)^2 d\tau > 0$, where $\phi\,(\tau)$ is a solution of the jet equation.

We thus obtain the first order expression for the modified free energy functional:

$$\mathcal{F} = \mathcal{F}_0 + RH_0 + R\left(e\,(u)\,L - 2u\int_{A_+} h(y)d^2\mathbf{r}\right) \tag{25}$$

We compute on the same way the first order area $\mathcal{A}$. As the jet solution $\phi\,(\tau)$ is even, if we choose $\phi\,(0) = 0$, there will be no jet contribution to $\mathcal{A}$ at this order. The only contribution will come from the first order modification of ϕ outside of the jet and will therefore be independent of the jet shape. We thus conclude that, at this order, the minimization of the free energy with the area constraint is equivalent to the minimization of (25) with a given area A_+. As the two first terms of (25) are constant, this new variational problem is a variational problem on the shape of the jet.

On one hand, if the topography is zero at first order, we observe that this variational problem corresponds to the minimization of the jet length for a given area. The jet are then straight (zonal bands separated by strong jets) or circular (circular vortex) (this is the equivalent of bubbles in first order phase transitions). Figure (4) shows the corresponding phase diagram with respect to the energy and to the asymmetry parameter B. On the other hand when a topography is present at first order, the tendency to minimize the jet length will be counterbalanced by the second term: the positive (resp negative) PV tends to concentrate on extrema (resp minima) of the topography. For a topography $h\,(y)$, the vortices will therefore be elongated in the zonal direction.

To give a quantitative description of this fact, we can obtain from the variational problem

(25), an equation describing the shape of the vortex. We refer to Bouchet and Sommeria (2002) appendix B, for the actual computation. The result is that the radius of curvature r of the curve formed by the jet (for instance the curve of value $\phi = 0$) must verify:

$$\epsilon u \left(h(y) - \alpha_1 \right) = e(u) \frac{1}{r} \tag{26}$$

where $\varepsilon = 1$ (resp $\varepsilon = -1$) for an anticyclone (resp cyclone) solution, and α_1 is a Lagrange parameter associated to the conservation of the area $\mathcal{A}$. This relates the vortex shape to the topography and parameter u. As said in the introduction of this section it is also possible to obtain such a result from the first order jet equation analysis. α_1 then turns out to be the Lagrange parameter appearing in the Gibbs state equation (17).

In appendix A we give equations which permit to numerically compute the vortex shape, from equation 26. Figure 5 compares the numerically obtained vortex shapes, with the Jovian ones. This shows that the solution to equation (26) have the typical elongated shape of Jovian vortices.

In appendix A, we also analytically compute the half width of the vortices y_m. For the cosine topography (4), we obtain :

$$y_m = \frac{1}{2} g \left(\frac{e\left(u\right)}{2au} \right) \tag{27}$$

where g is the inverse of the function $\sin x - x \cos x$ for $0 < x < \pi$.

From this formula, we see that the maximal latitudinal extension of the vortex solution is given by a typical length defined by the topography. We stress the important point that this maximal extension y_m is independent on the parameter B, or equivalently is independent on the area of the vortex. Varying this area, the only way for the vortex to extend is to be very elongated in the zonal direction. This very strong qualitative property of these equilibrium solutions is in agreement with the observed brown barges, as illustrated by figure 5.

A very strong property for the topography may be obtained from the equation for the jet curvature radius. For a vortex solution, latitudinally elongated, like the Jovian ones, the radius of curvature of the jet have its minimum value at the latitude of the center of the spot. From equation (26) we can then deduce that the zonal topography must have an extrema under the center of the vortex. Dowling and Ingersoll (1989) have analyzed the velocity field of the GRS and of the white oval in the Shallow-Water framework. They have then obtain the Shallow-Water topography. In Bouchet and Sommeria (2002), we have used these result to compute the Quasi-Geostrophic topography. Results are reported on figure 6. It clearly shows extrema of the topography under these two anticyclones.

If the effect of topography is strong enough: $e\left(u\right) / \left(au\right) \gg 1$, the vortex latitudinal extension will be much smaller than the typical variation length of the topography, we can then expand (27) around $y_m = 0$. The maximal extension of the vortex is then only determined by the curvature of the topography around its extremum (quadratic approximation). Let us parameterize this curvature by a_{qd} $\left(h\left(y\right) = -\varepsilon a_{qd} \left(y - y_0\right)^2 + h\left(y_0\right)\right.$, where y_0 is the latitude where h reaches its extremum, $\varepsilon = \pm 1$. For the cosine topography (4) $a_{qd} = 4a$.

The expansion around $y_m = 0$ yields:

$$y_{max} = \left(\frac{3e(u)}{2\epsilon a_{qd} u} \right)^{\frac{1}{3}}. \tag{28}$$

Using equation (26), we have described the vortex solutions. As an alternative, zonal solutions exist, in which two straight jets, flowing respectively eastward and westward, surround an area of small change of ϕ (shear flow). These jet positions may also be characterized by equation (26), when $1/r = 0$. Their latitudinal position $y_\pm$ is then determined by $h(y_\pm) = \alpha_1$. Their respective positions are thus symmetric with respect to the zonal extrema of the topography. The both type of solutions (jets or vortices) are then selected from the maximum entropy criteria, or equivalently maximizing the values obtained for the first order modified free energy (25). This selection depends on the parameters a defining the topography (4), on the domain aspect ratio, and on the two parameters u and α (equivalently the energy E and the asymmetry parameter B). In figure (7), we show the obtained phase diagram for a given value of a and aspect ratio, in the quadratic topography approximation. It shows a transition from vortex to jet solutions, when the asymmetry parameter is sufficiently close to zero. The aspect ratio of the vortices is also represented. We refer to Bouchet and Sommeria 2002 for a detailed discussion.

In the limit of small Rossby deformation radius, the maxima of entropy for a given PV distribution and energy, are formed by strong jets, limiting areas characterized by a weaker shear. Straight jets forming bands and zones, or vortex solutions, are both possible. The maximum entropy principle allows to select the type of solution for given parameters. The deep layer shear, the active layer shear, the shape of the vortices, and the strength of the jets are linked by the relations (24,28 and 23).

In next section (2.4) we discuss application of these results to the Jovian troposphere.

2.4 Jovian troposphere applications

In the previous sections, we have deduced all the flow properties for the statistical equilibrium, in the limit of small deformation radius. The qualitative properties of the vortex solutions are the one of the Great Red Spot : an annular strong jet, forming an oval shaped boundary, surrounding a quiescent core and admits a zonal shear. To our knowledge, this is the first model having these qualitative properties.

In this section, we want to describe the main hypothesis of such a model for Jovian vortices, and its limitations. We also stress the main physical consequences of our analysis. In section 2.4.2 we discuss the possibility to apply the model of the previous section to quantitatively describe the Great Red Spot. This discussion comes back on the hypothesis concerning the Potential Vorticity initial distribution, and on the limitations of the Quasi-Geostrophic model.

In the previous analytical analysis, we have studied equilibrium structures in the limit of small Rossby deformation radius. We have seen that this hypothesis leads to strong concentrates jets. For instance, we conclude that the actual small value of R, with respect

to the width of the Great Red Spot is responsible for its annular structure. For the case of other vortices, such as the White Ovals, or the north hemisphere Brown Barges, the small radius of deformation this limit is no more valid. In section 3, 4 and 5 numerical computations of the maxima of entropy under constraints, which reproduce the properties of these vortices. Nevertheless, the analytical analysis permits to qualitatively understand the dependence on the parameters of such vortices, and it has permit us to determine the parameter values for such vortices.

We discuss in section 2.4.3 some properties the zonal upper layer shear and the deep shear, obtained in the previous analysis, that should be of interest for Jovian vortices. We explain why such structures are obtained only for very energetic flows. In section 2.4.4 we discuss an alternative to the Rhine's scale to explain the typical vortex width. We conclude this section by recalling the main hypothesis of the statistical mechanics approach.

2.4.1 The effect of the Potential Vorticity distribution on the equilibrium structures

A fundamental issue is the hypothesis we made on the PV distribution. We have supposed an initial PV made of two types of PV. As argued in Bouchet and Sommeria (2002), this is a natural hypothesis in the context of a Jovian latitudinal band. Indeed, this could be the result of intense incoming thermal plumes, as recently observed by Ingersoll et al (2000): conservation of the absolute angular momentum during the radial expansion leads to a strong decrease of the local absolute vorticity, which comes close to zero. This means that in the planetary reference frame, a local vorticity patch with value $-f_0$ (the planetary vorticity) is created. The opposite vorticity is globally created by the subducting flow, but it is close to 0 due the much larger area.

Of course, even if a two-level approximation is natural, the real fine-grained PV distribution is not actually known, and an important issue is to study the dependence of the results on such a distribution. The knowledge of this distribution is equivalent to the knowledge of an infinity of constraints, the Casimirs. This is a major practical limitation of such a statistical mechanics approach (it is not a theoretical one). A natural way to proceed is to study a-posteriori the choice of the distribution, by comparison with observed flows. This is the way we have proceed, by studying the simplest case, the two PV level case, and by comparing the results to the Jupiter's structures. In the same spirit, Turkington, Majda and DiBattista (2001) have proposed to study a fine-grained PV distribution the centered gamma distribution, in order to study the effect of a skewness to the PV distribution. They have shown the importance of an anticyclonic skewness to obtain anticyclonic structures. This is consistent with our 2 PV levels description with $B > 0$, and with the observed anticyclonic forcing by incoming thermal plumes, as discussed above. Using this centered gamma distribution, they have obtained the oval shaped vortices and jets. These jets are not however strong jets, and they do not observe the ring structure of the GRS. Using our study, we may explain why their distribution is not suited to study Jovian vortices.

The thermal plume forcing products PV patches with vorticity of order $-f_0$. Their is no physical to expect another type of forcing to produce very large values of PV with respect to $|f_0|$. Moreover, the fine-grained distribution is conserved, and the extrema of the coarse-grained distribution can only decrease. This is thus very natural to considered a

PV distribution with compact support (values of the PV bounded). This is not the case of the centered gamma distribution, and this may have several consequences. Indeed, it can be proved (Robert and Sommeria 1991) that for any bounded distribution, the equilibrium relation between the PV and the stream function $q(\psi)$ must be strictly monotonic and tends to two maximum $q_{\pm m}$ (the maximum and the minimum of the PV initial distribution) value for ψ going to $\pm\infty$. As a consequence $q(\psi)$ must have at least one inflection point. The $q(\psi)$ relation then has the shape of a tanh at infinity, possibly with more than one inflexion point. This last property is not verified for the centered gamma distribution. This is however an essential property, as it is necessary condition to prove the existence of the equilibrium structures for any parameters. Moreover, as shown by the present study, the tanh like shape of $q(\psi)$ (it is equivalent to the existence of at least two minima of the area free-energy 16) is essential to obtain the phase coexistence and strong jet property of the Jovian vortices. Moreover, besides these physical and theoretical arguments, it corresponds to the observed $q(\psi)$ relation for the GRS, as shown by the figure 12 of Bouchet and Sommeria (2002). We thus conclude that PV distributions with compact support should be preferentially studied to model geophysical flows.

The problem of the knowledge of the PV distribution is not, however, a real limitation in the case of small Rossby deformation radius. We will indeed argue that the main property of the equilibrium structures are independent of the exact distribution, in this case. Let us suppose that the initial Potential Vorticity distribution is made of an infinite number of PV levels (not only two as supposed in the previous section), but with bounded PV. The statistical equilibrium will then be described by a monotonic function $q(\psi)$ reaching asymptotic extrema at the minimum and maximum PV levels (Robert and Sommeria, 1991). In most cases such a function will still be represented by a tanh like curve (one inflection point). We still can use the minimization of a free energy similar to (16). The function f_C determining this free energy will correspond again to the coexistence of two phases as represented in figure 2. The derivation described in the previous section is independent of the actual shape of the function f_C. We will then obtain similar equations for the strong jet (23), surrounding shear (24), curvature radius (26) and extremal extension (27). Only the u depending functions in these equations, will depend on the actual PV distribution. We recall that, as illustrated by the figure 12 of Bouchet and Sommeria (2002), a tanh-like shape is observed for the GRS.

We may also imagine a curve $q(\psi)$ with more than one inflexion point, instead of a single one, resulting in the coexistence of more than two phases. The most common case will be however a two-phase equilibrium. Likewise in usual thermodynamics the coexistence of more than two solutal phases is unlikely, even when many chemicals (equivalent to PV levels) are mixed. Nevertheless, we still can use the minimization of a free energy similar to (16). The function f_C determining this free energy will then correspond to the coexistence of three (or more) phases. Solutions can then be an anticyclone on a topography bump coexisting with a cyclone on a topography minima, both surrounded by a mean PV area. The jet structure of each of these vortices will then always be described by equations similar to the jet equation (23), curvature radius equation (26) and extremal extension equation (27).

We thus conclude that the qualitative structure of the statistical equilibrium is indepen-

dent of the actual PV distribution. This result is valid only when the Rossby deformation radius is small.

2.4.2 A quantitative model for the Great Red Spot

The relations obtained in the previous section between the topography, the maximum jet velocity, the jet width, the surrounding shear, and the vortex shape have been written in dimensional form, in Bouchet and Sommeria (2002). We have then shown that the actual observed values of these physical properties, for the Great Red Spot, can be matched with this model. This then allowed the determination of the Rossby deformation radius and of the topography curvature under the spot. This proves that a model of the GRS, by a statistical equilibria of the Quasi-Geostrophic model, with a quadratic topography, with an initial condition made of two values of the initial potential vorticity, can fit observations with precision.

We discuss further these hypothesis. The first one concerns the topography. We have shown that for any topography, the essential point is that it has an extremum under the spot. This is confirmed by observations (see figure 6). The hypothesis of a quadratic topography is then natural. In this article, we have studied the effect of a cosine topography. The main results are the same. However the actual value of the width of the vortex may be changed. Actually, we will numerically compute the velocity field of the GRS for a cosine topography in section 4, and the actual values of the Rossby deformation radius and of the topography curvature will slightly change.

Concerning the potential vorticity distribution, we have argued in section 2.4.1 that the qualitative description does not depends on the actual initial PV distribution. However, the quantitative description, for instance of the shape of the vortex, depends on it (via the u depending functions). For instance, we think that a model with another initial PV distribution, may also allow to fit observations with precision, leading possibly to slightly different values for the Rossby deformation radius or for the actual topography curvature.

The validity of the Quasi-Geostrophic model, and of the description of the Jovian troposphere by a single layer, are limitations of our model. The validity of the Quasi-Geostrophic model, for the GRS description, has been discussed by Dowling and Ingersoll (1989) and it was found reasonably good as a first approach. It is not fully accurate, for instance, the maximum value of the Rossby number has been evaluated to be 0.36 (near the jet maximum curvature) (Mitchell and collaborators, 1981). We note that an analysis of equilibrium states in the Shallow-Water model leads essentially to the same structure (Bouchet, Chavanis and Sommeria, 2003), as the one presented in the present work, with corrections due to ageostrophy.

2.4.3 Energy, zonal shear and topography

We have proven in section 2.3.4, that vortices are located on topography extrema. This has been verified using the GRS and White Oval data (see figure 6). In section 2.4.1, we have argued that, for any PV distribution, the relation linking the radius of curvature of the jet with the topography will be again (26), where only the u depending terms will be

changed. Our conclusion on the topography extrema is thus independent on the actual PV distribution.

In the following, we stress some important consequences of our analytical analysis, concerning the shear flow, which are also independent on the actual PV distribution. Equation (24) describes the shear outside of the jets. Using (19), it can easily proven that $1 - C(1 - u^2) < 1$. Thus the shear in the active layer $\sigma = d\mathbf{v}_x/dy$ is larger than the shear in the deep layer : $\sigma_d = R^3 d^2 h/dy^2$. Qualitatively, this may be seen as a consequence of the fact that positive Potential Vorticity will sit predominantly on topography bumps.

Let us give a justification on a more general ground, in order to argue that this result is independent on the PV distribution. . We first prove that any *statistical equilibrium, not zonal (a vortex for instance), must have an energy* $E > 0$. Let us consider a statistical equilibrium for any PV distribution. On one hand, it can be proven on a general ground, that for positive temperatures states $\beta > 0$, only one solution to the equilibrium state equation exist (see for instance Michel et Robert 1994a). On the other hand, in a periodic geometry, with topography, or in a channel geometry, it can be proven easily that a zonal solution exists (following Michel and Robert proof of the existence of the equilibrium, but restricting the study to a one dimensional equation). This proves that positive temperature states are zonal. Moreover, when only one state is possible in such maximization of entropy with a given energy, it can be proven that the inverse temperature β is a decreasing function of the Energy E (or equivalently that the equilibrium entropy is concave, see Bouchet and Barré (2003) for a justification). From this we deduce that all states with $\beta > 0$ have an energy lower than the state with $\beta = 0$. The only state with $\beta = 0$ is a completely mixed state: $q = 0$, thus $\psi(y) = R^3 h(y)$, and $E = 0$. We thus conclude that all equilibrium structures with energy $E < 0$ are zonal. Conversely, this proves that any statistical equilibrium, not zonal (a vortex for instance), must have an energy $E > 0$. We recall that we have supposed $C = -R^2\beta > 1$, in the analysis of equilibrium states (section 2.3). We note that this reasoning may be easily applied to any stable stationary state of the Quasi-geostrophic equation, with topography, in a channel or doubly-periodic geometry (by considering the functional which is minimized in the derivation of the first Arnold stability theorem (Arnold 1961)). We also note that this result is independent off any hypothesis on the PV distribution and on the value of R. When the PV distribution is known a-priori, the critical value β_c of β (resp the Energy) below (resp above) which non zonal solutions may exist, may be proven to be strictly positive. For instance, for the two-level distribution we have considered, it can be proven that $\beta_C > 1/R^2 + \lambda_1$, where $\lambda_1$is the first eigenvalue of the Laplacian, for the geometry considered. [3].

We end this discussion, by qualitatively linking this result, with the strength of the shear. We first note that in the Quasi-Geostrophic model, PV interacts mainly with PV values at a distant do lower than a typical length of order R. This allows to conclude that negative PV patches on topography trough lower the Energy (and conversely for positive PV patches). As a consequence, in any state with $E > 0$, positive PV must dominate negative PV on topography bumps. The shear in the upper layer is thus larger than in the lower layer.

We have proven that stable stationary flows, not zonal (a vortex for instance), must have

[3]This criterion is linked with the hypothesis of the second Arnold stability theorem.

an energy $E > 0$. This has a strong practical implication : to numerically obtain vortices like the Jovian ones, with small values of R, one has to start with an initial conditions where positive PV dominate negative PV on topography bumps.

2.4.4 An alternative to the Rhines' scale

For a geostrophic turbulence with a linear β effect ($h(y) = \beta y$), it has been argued that typical length for the vortex size should be $L_\beta = \pi\sqrt{U/\beta}$ (the Rhines' scale, Rhines and Young 1982), where U is a typical flow velocity. On the contrary, when the value of the Rossby deformation radius is small, for a strictly linear beta-effect, the statistical equilibrium vortex solution are circular, with jet width scaling with, but without limit to their size, due to the beta-effect. The beta-effect is only responsible for a constant westward velocity drift such as to compensate the beta-effect (see Bouchet and Sommeria 2002).

When a more complex topography is taken into account (not linear), our study in section 2.3 has shown that the vortex width has a maximal value. The maximal latitudinal extension for a zonal topography is for instance given by (27) for a cosine topography or by (28) for a quadratic topography. We thus deduce from this analysis that a typical vortex width is related to the topography curvature, and not to the topography first-derivative, as in the Rhines' scale case. The topography curvature is itself directly related to the shear surrounding the vortex (24) or to the deep shear. We obtain the following dimensional typical latitudinal extension for the vortex $L_\sigma = \left(R^2 U/\sigma_d\right)^{1/3}$, where U is the typical strong jet velocity, and σ_d is the deep shear, of the same order as the shear surrounding the vortex or. If we moreover consider that the typical potential vorticity is of order $|f_0|$, the planetary vorticity, and that the jet width scale with R, we obtain $U \propto R\,|f_0|$. This gives an other expression of the typical latitudinal extension in terms of the Rossby deformation radius and on the shear : $L_\sigma = R\left(|f_0|/\sigma_d\right)^{1/3}$. As R, $|f_0|$ and σ_d are independent on the initial conditions (PV distribution and energy), the typical latitudinal extension is independent on the forcing. We recall that the exact value of the latitudinal extension, for a given PV distribution and energy, for a given topography, may be computed from the small R expansion (27 or28), or numerically for larger values of R.

2.5 Relaxation equations : a small scale turbulence parameterization

As discussed in the beginning of this section, the equilibrium statistical mechanics describes the states of optimum Potential Vorticity mixing, for a given energy and PV distribution. The dynamics of the Quasi-Geostrophic equations (1) should be responsible for such a mixing. From a numerical point of view, the correct parameterization of this mixing is a crucial issue for the modeling of geophysical flows. Accordingly to the ideas of statistical mechanics, Robert et Sommeria (1992) have proposed a parameterization of turbulence, for two-dimensional or Quasi-Geostrophic flows, based on a Maximum Entropy Production Principle (MEPP). The corresponding equations have the property to maximize the entropy production while conserving all the dynamical invariants. As they converge, for infinite time, towards entropy maxima, they have been called relaxation equations. Therefore, they can also be used to numerically compute maxima of the entropy for given PV distribution and energy.

Let us present these equations in the context of the Quasi-Geostrophic dynamics. In the following sections we will use them for dynamical simulations. We will show their interest, compared with other parameterizations, to perform flow simulation (section 3.3). We also use them to compute equilibrium structures that we will compare to the actual vortices of Jupiter troposphere (sections 3, 4 and 5).

Relaxation equation may consider any potential vorticity distribution (Robert and Sommeria 1992, Robert et Rosier 1996). However, for sake of simplicity, we consider a situation for which the initial condition is composed only of PV patches of vorticity a_1 and a_{-1}. This choice is in accordance with the equilibrium structure analyses, presented in sections 2.2.2 and 2.3 We have argue in section 2.4.1 that the qualitative properties of the equilibrium structures are not affected by the PV distribution, for sufficiently small Rossby deformation radius. Once this simplification is assumed, the relaxation equations are (Robert and Sommeria 1992):

$$\frac{\partial \omega}{\partial t} + \mathbf{u}.\nabla\omega = \nabla.\left(\nu\left[\nabla\omega + \beta\left(a_{-1}-\omega\right)\left(\omega - a_1\right)\nabla\psi\right]\right) \tag{29}$$

with

$$\beta = -\frac{\int_D d\mathbf{r}\,\nu\nabla\omega.\nabla\psi}{\int_D d\mathbf{r}\,\nu\left(a_{-1}-\omega\right)\left(\omega-a_1\right)\left(\nabla\psi\right)^2} \tag{30}$$

where β is the Lagrange parameter associated to energy conservation and ν is a turbulent viscosity. The first term of the right hand side of equation (29) is a usual diffusion. The second term on the right hand side of (29) is a drift term which acts to maintain a constant energy. Accordingly to the MEPP hypothesis, it is derived such that the entropy production is optimal.

In section (3.3), we will consider numerical simulation using only a viscosity, this is the usual eddy diffusivity hypothesis. We will then show that such a parameterization is unable to reproduce even the qualitative properties of the flow, for very long time simulations. In both cases, relaxation equations and eddy viscosity, we will use the minimal value of ν, compatible with a given resolution. We note that there is no theoretical ground to assert that the coarse-grained dynamics should be such to maximize the entropy production. The relaxation equations (29) are however likely to better describe the dynamics because, on one hand, they respect the conservation laws of the inertial dynamics, and in the other hand, they take into account the tendency towards mixing of the system.

We note that a numerical algorithm to compute maxima of entropy under constraints, which does not use relaxation equations, is described in Turkington and Whitaker (1996).

3 White Ovals formation from randomly distributed vortices.

In this section and in the following ones, we use the relaxation equations, presented in section 2.5, to simulate an inertial dynamics and/or to compute the statistical equilibrium of the Quasi-Geostrophic model.

As a first experiment, we show in section 3.1, how potential vorticity patches with random positions, lead to the formation of several vortices, which progressively merge until

forming a unique structure. Due to the presence of a topography, these structures have an elongated shape. The parameters have been chosen to make an analogy with the Jupiter's White Oval flow.

In section 3.3 we compare such a simulation with a Direct Numerical Simulation (usual viscosity).

3.1 Anticyclones formation from randomly distributed vortices

Let us consider the evolution of an initial condition formed by anticyclonic potential vorticity patches, randomly distributed (figure 8). The resolution of this computation is 512x128. Parameters are $R = 0.2$, $a = 0.4$, $a_1 = 4.2$, $a_{-1} = -1$. We use a diffusivity $\nu = 1.5\,10^{-4}$. The time step is $\Delta t = 6.13\,10^{-3}$.

Figures 8 and 9 illustrate the evolution of this initial condition, modeled by relaxation equations. They show the coalescence of the vortices, progressively forming several anticyclones, in a latitudinal band limited by topography. Any of these anticyclones is then centered on the topography maxima, located in the center of the picture. These anticyclones form local statistical equilibrium, as illustrated the scatter-plots of the potential vorticity versus the stream function, on figure 9.

Time lapses between pictures of figure 8 correspond to few turnover times (16 from first to last). The local organization is thus very rapid. On the contrary the time lapse between the two last pictures of figure 9 is approximately of 50 turnover times. During this time, the two anticyclone have progressively achieved a local equilibrium as illustrated by the sharpening of the two curves on the scatter plot of potential vorticity versus stream function. Their respective position is however quite unchanged.

Let us recall that the deformation radius value is $R = 0.2$, which is very small compared to the latitudinal band length : 4π. As the interaction between the two vortices decrease exponentially for values greater than R, it is in this case very small. This explains the very long time needed for the system to achieve the exact equilibrium structure. After a much greater time lapse (approximately 300 turnover times) the two anticyclones finally coalesce, to form a unique structure, visible on figure 10.

3.2 The White Ovals evolution and structure

The three White Ovals at 33^o S, called BC, DE and FA, where the larger anticyclones on Jupiter, after the GRS. They formed when an anticyclonic zone broke into three parts in 1939-40 (see Ingersoll and collaborators 2002 for references). In 1998, the anticyclones BC and DE merge into a larger one. This new oval then merge with the oval BA in 2002.

This behavior is predicted by the statistical mechanics. The quick organization into oval shaped vortices, followed by a very long time before the three ovals actually merge in a single structure is very similar to the one described in the previous computation (figures 8, 9 and 10). In this last case, these vortex have emerged from random initial patches. However as illustrated in section 13, the same structures could have been obtained from the destabilization of jets.

The equilibrium velocity field (figure 10) then shows a structure very similar to the white

ovals ones: the anticyclone is too small for the limit of small Rossby radius R to apply. As a consequence we do not observe a quiescent inner region as is the case for the Great Red Spot. The anticyclone has nevertheless an oval shape, linked to the deep flow shear and to the upper layer shear. We have not given dimensional values for the quantitative characteristics of this equilibrium structure, nor tried to match them by choosing appropriate values of R and of the topography curvature. This may however be done, using an iterative scheme, as we will describe in the following section, for the Great Red Spot.

Such a work would be of special interest, in order to try to use the observation data from the observation of the merger of these anticyclones (see for instance Sanchez-Lavega and collaborators 2000). One could first put some constraint on the physical parameters by using the actual properties of the spot before merging, and verify the large anticyclone after merging is compatible with statistical mechanics predictions.

3.3 Comparison of relaxation equations with usual eddy-diffusivity parameterization

Figure 11 shows vorticity fields obtained after 25 turnover times, either using eddy-diffusivity or the relaxation equations, using in both cases the same resolution 512x128. Even if the time elapsed from the beginning of the computation is very small compared to the global organization time, this figure shows important qualitative differences between these two modelings. The vorticity patches are far less compact for eddy-diffusivity type computations. Moreover the decrease of energy is already important for this last computation. These differences are crucial for long time dynamics : the eddy-diffusivity type computation indeed rapidly leads to a complete energy dissipation. As a consequence, a numerical experiment, with an eddy diffusivity, showing the formation of anticyclones from random initial vorticity patches and their vary slow evolution towards a final unique vortex (as show on figures 8 and 9) is probably infeasible.

As explained above, this is mainly due to the small value of the deformation radius R, for which the dynamical organization is very slow. This illustrates very clearly the interest of the relaxation equations in such a context.

4 The Great Red Spot of Jupiter.

4.1 A model of the Great Red Spot

Let us propose a model of the Great Red Spot of Jupiter, as a statistical equilibrium structure. We model the latitudinal band of the Great Red Spot as a periodic domain of latitudinal extension $L^\star = 18\,800\,km$ and longitudinal extension $4X18\,800\,km$, with a zonally periodic topography of the same periodicity. As explain in section 2.4.3, the organization of the structure is essentially local and determined by the topography under the vortex. Thus the artificial boundary conditions used here, are of no importance (due to the small value of R, the equilibrium structure for a wider and more elongated latitudinal band will be only slightly different from the one computed here). We use the following parameters : $R^\star = 1460\,km$, $a^\star = 1.3\,10^{-16} km^{-3} s^{-1}$, $a_1^\star - a_{-1}^\star = 2.14\,10^{-4} s^{-1}$ (the corresponding dimensionless parameters are $R = 0.234$, $a = 0.117$, $B = 0.87$, $u = 0.99$). We numerically

compute the equilibrium structure corresponding to these parameters, using the relaxation equations described in section 2.5.

Figure 1 shows the potential vorticity and the velocity field for the equilibrium structure, as well as the velocity field obtain from Voyager data analysis (from Dowling and Ingersoll 1998). Let us note the very good qualitative agreement between the two velocity fields. We have numerically computed the parameters of this vortex : the maximum jet velocity is $v^\star_{max} = 120\, ms^{-1}$, the jet width (length between the two points where the jet velocity is half of the maximum jet velocity) is $l^\star_x = 3600\, km$ for the jet at mid latitude (flowing northward or southward) and $l^\star_y = 2900\, km$ for the extremal latitude jet (flowing eastward or westward), the maximum latitudinal extension (length from the center of the vortex to the point northward, where the jet achieves its maximal speed) is $y^\star_m = 3800\, km$, the aspect ratio of the spot (the length is measured using maximum jet velocity point, as for $y^\star_m$) is $\delta = 1.8$, and the surrounding shear is $\sigma^\star = 0.5\, 10^{-5}\, s^{-1}$

All these quantities are compatible with the observed ones (data from Mitchell and all 1981 analysis), except for the surrounding shear whose real value is $\sigma^\star = 1.5\, 10^{-5}\, s^{-1}$. We thus conclude that the statistical equilibrium of the 1-1/2 Quasi-Geostrophic model, with a cosine topography and with a 2 level PV distribution, allows to model quantitatively all the main characteristics of the Great Red Spot, except for a factor 3 for the shear.

A natural question is whether this result could be improved in the context of the 1-1/2 Quasi-Geostrophic model. To obtain the above parameters, we have used the indications given by the relations (23,24,27) and the computation of the maximum jet velocity, in order to design an iterative scheme to find the parameter best suited to the modeling of the Great Red Spot. As this scheme converged, we do not think that it could be better with the same topography and the same PV levels distributions. An analysis of equations describing the vortex shape (26,27) either for a quadratic or for a cosine topography, shows that a quadratic topography should give better results. This is consistent with the study of this last case in Bouchet and Sommeria (2002). Concerning the choice of the PV distribution, we have argued in section 2.4.1 that a different PV distribution, compatible with a $q - \psi$ with a concavity change, would give similar results with different values for the u depending functions in the relations (23,24,27) . This may be a way of improving these results.

However, our feeling is that such a search for improvement is of little interest, given that the 1-1/2 Quasi-Geostrophic is a crude model of the troposphere of Jupiter. Firstly, the geostrophic balanced is not well verified in the area where the curvature of the jet is minimal, and the layer height variations are not very small compared to the layer height. A 1-1/2 Shallow-Water model would improve the results, and be more convenient to make a very precise study. Secondly, a 1-1/2 layer is certainly a crude approximation of the Jovian troposphere.

4.2 Validity of the lower order approximation

The model we propose assumes several hypothesis (PV distribution, optimal mixing) and approximations (for instance the Quasi-Geostrophic model 1-1/2 model). This numerical computation allows to test the approximation made when describing the solution by its lower

order description when $R \to 0$. For instance, for the width of the jet, we have obtained $l_x^\star = 5100\,km$ and $l_y^\star = 4100\,km$. The jet width thus depends on latitude (this is visible on both the computed and the observation velocity fields, figure 1) and is larger than the first order prediction. This is a consequence of the shear (for $l_y^\star$) and of the strong curvature of the jet near the extrema of the topography (for $l_x^\star$). There, the curvature r is only 3 times the Rossby deformation radius R, which limits the validity of the approximation $R \to 0$. We note that the latitudinal dependence is present at the following order of the asymptotic expansion (see Bouchet 2001, part 1, section 4.3).

We also note that the curvature at mid latitude is greater for the numerically computed equilibrium than the analytical prediction. This is also due to the small R approximation. This curvature difference in this area is important, however this has only a limited effect on the maximal latitudinal extension of the spot. Indeed, the value y_m analytically predicted is $y_m = 4300\,km$, whereas the numerically computed one is $y_m = 3800\,km$. This explain why the shape of the spot is correctly predicted by the analytical relation, in spite of the limitations of the lower order approximation. The curvature of the real jet is also smaller than the one of the numerically computed one. This may be due to the discrepancies of the Quasi-Geostrophic approximation in this area (cyclostrophic balance).

We thus conclude that the lower order of the small Rossby deformation radius is valid only as a first approximation, for a value of R corresponding to the GRS (let say 30% for the described variables). However, we note that the qualitative agreement is very good. In particular, the prediction of the latitudinal maximal extension, and of the vortex shapes is good. Whereas the numerical values are not exact, this analysis has permitted us to understand the role of the various parameters, in order to find parameters suited to model the GRS, the White Ovals (section 3) or the Brown Barges (section 5).

5 Thermodynamic phase transition and strong jet stability.

Because of the very different typical time scales, for forcing and dissipation in on hand, and for inertial organization in the other hand, Jupiter's features appear stationary. For instance, the Great Red Spot is observed from more than three centuries. Whereas its length seems to have change during this time, its global structure is likely to be the same. Jovian feature should therefore be stationary for the inertial dynamics.

A large amount of work has dealt with the stability of quasi-two dimensional flows. Linear stability of jets has been for instance addressed by Rayleigh, Kuo, Charley and Stern (see Pedlosky (1987) for a discussion for geophysical flows). Nonlinear stability results have first be obtained by Arnold (1966) for the Euler equation. The flows are then proven to be stable because they minimize a functional, built on the Casimirs and on the energy, invariant under the dynamics (formal stability). A further estimate on this functional allows to prove that a perturbation around the stationary state remains bounded under the nonlinear dynamics (non-linear stability). A generalization of these ideas for other flow equations have then been studied (see for instance Holm and collaborators (1985) or Yongming, Mu and Sheperd (1996) for geophysical flows). In the case of zonal solutions, for the Quasi-Geostrophic equation or for the Euler equation, the linear stability results can be retrieve from the nonlinear stability results.

These stability results are only sufficient condition for stability. Lots of geophysical flows, essentially the most energetic ones, are indeed stable whereas they do not verify the hypothesis of these theorems. For the Jovian atmosphere, this is for instance reported in the review of Dowling (1995). This has led to some interrogation on the stability of these flows. These questions have been emphasized also by the difficulty to obtain numerical model of such flows, having strong jets, typical of the Jovian troposphere.

The statistical mechanics of the potential vorticity offers a way to understand this stability. The link between the Arnold's stability theorems and the statistical equilibrium has been noted for instance by Robert and Sommeria (1991) (see also Bouchet (2001)). In such works the equivalent of the Arnold's theorem hypothesis is that only one solution exist for a given inverse temperature β. This has been proven for states with $\beta > \beta_c$ (or equivalently for energy sufficiently small $E < E_c$, as proven in section 2.4.3). For smaller β (larger energy $E > E_c$), the stability of the flow was qualitatively understood by the impossibility of the potential vorticity to mix further. A clear formalization of this statement has been proposed recently by Ellis, Haven and Turkington (2002), where an augmented functional, taking into account of the Energy conservation, have been used to generalize the Arnold's stability theorem. The result of this work is that any entropy maxima under constraints, except the ones close to a phase transition point, is stable. As no norm is specified in this work, and the a-priori estimate necessary to prove a nonlinear stability theorem is not provided, these results are the proof of formal stability (see Holm and collaborators (1985) for a precise definition of formal stability) of such flows. This is however a decisive step towards the understanding of the stability.

A crucial hypothesis needed to use these results is that the second variations of the augmented functional used by Ellis, Haven and Turkington (2002), be definite positive. In Ellis, Haven and Turkington (2002), this point is not analyzed in details, and cited as a technical problem. Unfortunately, this is not right in most of the situations. As soon as the equations have some symmetry, and the flow does not respect this symmetry, the second variations can not be definite positive. At least one direction must have a zero eigenvalue. For instance, in our case, the vortex solutions break the zonal symmetry. A small perturbation of such a vortex, can lead to the translation of the vortex by a finite distance. For this reason, a nonlinear stability result is not possible. However, the situation is physically very clear: a perturbation can only lead to flows close to the initial ones, up to an arbitrary translation. A clear formalization of these ideas remains to be done. Anyway, the results of Ellis, Haven and Turkington (2002) are a decisive step towards the understanding of the stability of such flows.

Statistical equilibrium are thus stable, as soon as they are not too close to a phase transition. On a practical point of view, one thus have to study the phase diagram of the equilibrium states. For instance phase diagrams on figure 4 and 7 represent stable stationary flows, similar to Jovian vortices and jets. Please note that some other stable states may exist for the same energy and parameter B (metastable states, for instance).

As illustrated on figure 7, depending on the parameters, strong jets or vortex solutions may be stable, depending on the values of the parameters E and B. In order to illustrate these stability properties, we consider the evolution of an initial condition composed of an anticyclonic PV band, standing on the maximum of the topography. The corresponding flow

is made of two strong zonal jets flowing eastward and westward respectively. The PV has a width l. We strongly perturb this initial condition by centering the PV band on a latitude y_c varying with the longitude: $y_{centre} = \pi/2 + l/4 \sin x + l/12 \sin(3\pi/2 + \pi/6)$. Figures 12 and 13 show this initial condition, for $l = 1.09$ and $l = 0.31$ respectively. The values of the topography parameter (see 4) and of the Rossby deformation radius are $a = 0.6$ and $R = 0.25$ respectively.

The parameters for the numerical simulation are $\nu = 5.93\,10^{-5}$ (resolution 512X128), corresponding to a Reynolds number (based on the Rossby deformation radius) of $Re = (Rv_{max})/\nu$ equal to 820. The numerical time step is $\Delta t = 0.012$.

Figure 12 illustrates the evolution for the first initial conditions. The first picture show that the two jets, are destabilized by this strong perturbation. The jet however stabilize accordingly to the phase diagram on figure 7 (the value of B is then close to zero). We note that this initial condition does not verify the non-linear or linear stability theorem hypothesis. The last of these pictures show slight oscillations of the PV level lines, that we interpret as Rossby waves, guided by the jet. The relaxation of these waves is very slow.

Figure 13 illustrates the evolution, for the second initial condition. As the area of the PV band is then small, the value of B is no more close to 0. Accordingly to the phase diagram on figure 7, the two jet destabilize and form anticyclones. The statistical equilibrium is then an elongated anticyclone centered, on the topography extrema. The final state is shown on figure 14. This solution will also be used in next section to model one of the cyclonic Brown Barges of the Jupiter's north hemisphere.

6 The north-hemisphere Brown Barges

Brown Barges are brown oval spots (see figure 5), located at 14^o N on the Jupiter's troposphere. On the contrary to most of Jovian features, these vortices are cyclones. A study of these spot velocity field is reported in Hatzes and collaborators (1981). In this section, we model this spot with the statistical equilibrium vortex obtained in the previous section, from the destabilization of a strong jet (figure 13). We compare the velocity field of this statistical equilibrium structure with the data analysis of Hatzes and collaborators (1981).

The equilibrium PV field obtained from this numerical simulation is represented on figure 14. This figure actually represents an anticyclone. However, because of the symmetries of the Quasi-Geostrophic model, a symmetric cyclonic structure may be obtained. The very elongated shape, with a maximum latitudinal extension may be compared to the image of one of the real Brown Barges (see figure 5). We also represent the velocity in a latitudinal and meridional sections of the spot, both for the statistical equilibrium and for the data analysis of Hatzes and collaborators (1981). One may observe that the velocity structure is the same. The northward velocity, along a meridional section, shows a strong jet structure at the front edge of the spot, whereas it is null inside of the spot. On the contrary, the eastward velocity along a zonal section, does not show the jet structure : it is essential a shear flow. The comparison of these plots shows that statistical equilibrium describe very well the qualitative properties of this spot. We have not tried to give some dimensional values of the main characteristic of the spot. However this could be done. By an iterative algorithm, one could then try to predict the actual values of the topography curvature and

of the Rossby deformation radius, as we have done for the Great Red Spot.

The structure is thus different from the Great Red Spot one's. The jet structure on the northward velocity allows to conclude that the Rossby deformation radius is small. The effect of a very intense topography curvature characterizes the Brown Barges. For this reason, the topography can no more be treated as a first order perturbation, like has been done in section (2.3). However, an asymptotic description, following the same ideas can be done, assuming the amplitude of the topography as having effects on the zeroth order of the asymptotic expansion. The result is a modified algebraic equation describing the velocity field outside of the spot. The jet structure then explicitly depends on the latitude y. The shape of the vortex is always described by an equation similar to (26). However, the dependence on y because of the topography, is no more due only to the PV variation inside of the spot, but also to the latitudinal dependence of the jet properties. We leave a more precise description and study of this asymptotic expansion for future works.

In Hatzes and collaborators (1981), authors insist on the oscillations of the shape of this cyclone, whereas we have described only a stationary solution, with similar velocity field structure. We note that, as in the case of the jets described in section 5, perturbation of the equilibrium structure would lead to oscillations around the stationary flow which should describe the observed ones. A further study of this problem may be of interest.

7 Conclusion

We have described equilibrium of the potential vorticity statistical equilibrium, for the Quasi-Geostrophic equation. Independently of the statistical interpretation, all the flow we have described are stable stationary flow for the inviscid dynamics. We have first presented results in the limit of small Rossby deformation radius. The main ideas of this asymptotic description are present in the work Bouchet and Sommeria (2002). The derivation proposed here is however simplified. We have discussed in details the generalization of these results to any potential vorticity distributions. Using numerical computations, we have also described statistical equilibrium flows for parameters for which the hypothesis of a small Rossby deformation radius no more holds. The application of these results to model, the Jovian strong jets and main vortices are extensively described.

In the limit of small Rossby deformation radius, the equilibrium flows are characterized by strong jets. The minimization of the entropy selects either zonal solutions or vortices bounded by strong jets, depending on the parameters. These jets play the role of an interface separating two area of different potential vorticity mixing. The shape of this interface is given by the minimization of their length, for a given area. Under the presence of a deep zonal flow and of a beta-effect, or equivalently of a topography, this minimization is balanced by the tendency of anticyclonic potential vorticity to stand around the maxima of the topography. This leads to the characteristic elongated vortices observed on Jupiter's troposphere. The width of these vortices may be computed exactly. A typical width is given by an alternative of the Rhine's scale, built on the curvature of the topography, or equivalently on the deep layer shear σ_d : $L = (RU/\sigma_d)^{1/3} = R\,(\Omega/\sigma_d)^{1/3}$. This model predicts that vortices sit on extrema of the topography. This property has been verified using available data for the Great Red Spot and the White Oval BC.

Using these results, we have proposed a quantitative model for the Great Red Spot. In Bouchet and Sommeria (2002), using the small Rossby radius derivation, with a two PV-levels distribution, we have shown that an appropriate choice of the energy, total potential vorticity, topography curvature and Rossby deformation radius allows to reproduce the observed jet maximum velocity, jet width, vortex shape and aspect ratio, and surrounding shear. In this work, by comparison with numerical computation of the equilibrium, we have shown that the small Rossby radius approximation leads to a correct description of the structure of the vortex, for the Great Red Spot parameters. The discrepancies due to finite size effects are of the order of the error due to the Quasi-Geostrophic approximation. The obtained velocity field compares very well with the observed one.

Using numerical determination of the equilibrium flows, we have proposed models of the White Ovals or of the cyclonic Brown Barges. These vortices may be obtained either from random initial conditions or from the destabilization of strong jets. The White Ovals are characterized by a size which is of the same order as the Rossby deformation radius. The deep shear is responsible for their oval shape and for the surrounding shear. The Brown Barges are characterized by a very strong topography curvature. For these vortices, we have obtained their typical jet like structure for the northward velocity in a zonal section, and their typical shear for the eastward velocity in a meridional section.

The statistical mechanics predicts some strong qualitative properties for Jovian like vortices. For a given deep shear, and Rossby deformation radius (for the same latitudinal band, for instance), smaller vortices are close to a circle. Their aspect ratio grows with the size. The latitudinal extension of the spot as a maximum value, forcing a very elongated shape as the one of the Brown Barges. For such vortices to exist, a critical energy in the latitudinal band must be present. When this is the case, the shear in the active layer has to be larger than the shear in the deep layer. Vortex adapt their zonal drift speed, such as in their reference frame, they are located in an extrema of the topography. Thus similar vortices in the same latitudinal band must have a relative zonal velocity if they are not located at the same latitude. This drift velocity is linear with the latitude difference, as soon as the latitude difference is sufficiently small for the deep shear to be supposed constant.

All the statistical equilibrium are dynamically stable, even when the conditions for linear or non-linear classical results do not apply.

The statistical mechanics of the potential vorticity describes the most probable flow for a given energy and potential vorticity distribution. The main assumption of this work is that such flows describes actually the observed jets and vortices of Jupiter's troposphere. The dynamical system ergodicity would be a sufficient condition to justify this hypothesis. The proof of ergodicity is very difficult, even for very simple dynamical systems. The best way to study the validity of statistical mechanics in complex systems remains the comparison of its predictions with observations of with numerical simulations. This works has shown that the statistical mechanics of the potential vorticity is able to model the main Jovian features and to predict important qualitative properties, which can be verified.

In a latitudinal band, the topography forces a shear flow in the active layer. This favors vortex merging, and thus the potential vorticity mixing. On the other hand, if we consider a topography with two bumps, following the same ideas as in this work, we

may for instance describe stable solutions corresponding to two anticyclones on each of the topography bumps. In these two bumps are of different high, this solution may not be a statistical equilibrium state, but only a local maxima of the entropy under constraint. In such a case, the topography would act as a dynamical barrier, preventing a real ergodicity for the system. However, the statistical interpretations would still remain clear.

An other point to be discussed is the slowing down of the dynamics, due to the small value of the Rossby deformation radius. The interactions between vortices, decays exponentially for distance much larger than R. For this reason, well separated vortices mainly not interact. This may prevent their merging predicted by statistical mechanics. It will at least impose a very long time scale to observe an effective ergodicity. This situation is illustrated by the merging of the three White Ovals which formed in 1938 (Sanchez-Lavega and collaborators 2000). The two last ones have finally merged in 2002, after a very long coexistence in the same latitudinal band.

Besides these qualitative arguments, we want to stress that ergodicity may really be questionable in some situations, for such systems. As an example we refer to Barré and collaborators (2002). In this study, a system with long range interactions, sharing deep analogies with quasi-two-dimensional flows, is shown to have very long lived out-of equilibrium states.

We have discussed some limitations of these statistical models for Jupiter's jets and vortices. The major ones concerns the validity of the modeling of Jupiter's troposphere by the Quasi-Geostrophic model. Whereas it is good as a first approximation, generalization of these results for a Shallow Water dynamics or for multi-layered dynamical models should provide more precise results in order to propose more precise comparison with the observed structures.

Some further studies of the equilibrium structure should be of interest to put precise constraint on the physical parameters. For instance, it may be possible to determine the deep shear under major vortices, such as the White Ovals or the Brown Barges. A model of White Ovals merging based on statistical mechanics could also permit to put further constraints on the physical parameters and potential vorticity distribution. Studies of linear perturbations around the equilibrium structures should be able to describe the spot shape oscillations, as observed for instance for the Brown Barges (Hatzes and collaborators, 1981).

In this work, we have assumed an inviscid dynamics. This is a very natural assumption, given the very different time scales for forcing and dissipation in one hand, and inviscid organization in the over hand. Whereas the observed features should be inviscid statistical equilibrium, the actual PV distribution and energy actually depends on the forcing and on the dissipation. We have for instance argued for a distribution with bounded potential vorticity, which should be well approximated by a two level distribution, because of the observed forcing by incoming thermal plumes. However, in order to go further in the analysis of the potential vorticity fine-grained distribution, one should model more precisely forcing and dissipation. This could permit to explain observable phenomena, such as the diminution, on a very long time scale, of the size of the giant anticyclones, or an eventual inviscid evolution of the oscillations of some vortices. In practice, the forcing should be introduced in kinetic like equations, like those developed in Kazantzev and collaborators, or following ideas described in DiBattista, Majda and Grote (2001). Such models would

explain the long term evolution of the fine-grained PV-distribution, whereas the observed structure should remain close to equilibrium structure during the evolution.

Acknowledgments

This work is part on the PHD thesis of F. Bouchet, directed by R. Robert and J. Sommeria. The first part of this work (Bouchet and Sommeria 2002), has been done in collaboration with J. Sommeria. The authors thank J. Sommeria, R. Robert and P.H. Chavanis for useful comments on the present work. During this work, one of us has been funded by a "Bourse Lavoisier" of the French "Ministère des Affaires Etrangères", and by the program COFIN00 "chaos and localization".

A Analysis of the jet shape equation

In section 2.3, we have obtain the equation verified by the jet position (26): $\epsilon u \left(h(y) - \alpha_1\right) = \frac{e(u)}{r}$. In this section, we discuss equations allowing numerical integration of this equation and we derive an analytical expression for the latitudinal extension of a vortex solution. This derivation, is a generalization to a cosine topography, of results in Bouchet and Sommeria (2002).

We look at anticyclones solutions ($\varepsilon = 1$) around the maxima of h (4). This extrema is reached for $y = \pi/2$. We make a latitudinal translation such that the maxima of the topography be on $y = 0$. We thus consider the topography $h\left(y\right) = 2a\cos\left(2y\right)$. The cyclone case may be easily recovered by symmetry.

To make the equation for the radius of curvature more explicit, let us define s a curvilinear parameterization of our curve, $\mathbf{T}(s)$ the tangent unit vector to the curve and $\theta(s)$ the angular function of the curve defined by $\mathbf{T}(s) = (\cos\theta(s), \sin\theta(s))$ for any s. Then the radius of curvature r of the curve is linked to $\theta(s)$ by $1/r = d\theta/ds$. This yields the differential equations :

$$\frac{d\theta}{ds} = \frac{2au}{e\left(u\right)}\cos\left(2y\right) - \alpha_1 \tag{31}$$

$$\frac{dy}{ds} = \sin\theta(s) \tag{32}$$

$$\frac{dx}{ds} = \cos\theta(s) \tag{33}$$

For symmetry reasons, it is easily verified that the solutions of (31, 33 and 32), with initial conditions $\theta(0) = \frac{\pi}{2}$, $y(0) = 0$ and some $x(0)$ are periodic. The resulting vortex is then symmetric with respect to the latitude of the maxima of the topography (here $y = 0$). Moreover, we have proved in the appendix C of Bouchet and Sommeria (2002) that these initial conditions are the only ones leading to vortex solutions (closed curves), in the case of a quadratic topography. The argument used there only uses the symmetry of the topography with respect to the extrema of the topography and can easily be generalized in the present case.

Let us compute y_m, the maximal latitude of the vortex (the maximal latitude of the jet center) (y_m is the half of the latitudinal extension of the vortex). We first note that the two variables θ and y are independent of x. We will therefore consider the system formed by the two first differential equations (31,32). It is easily verified that this system is Hamiltonian, with θ and y the two conjugate variables and

$$H \equiv \cos\theta + \frac{au}{e(u)} \sin(2y) - \alpha_1 y \tag{34}$$

the Hamiltonian. Thus H is constant on the solution curves. From the initial condition, we deduce $H = 1$. We note that for $y = y_m$, the curvature of the jet is 0 ($1/r = 0$). From 31, we thus obtain $\frac{2au}{e(u)} \cos(2y_m) - \alpha_1 = 0$. Combining this relation with the one obtained by using that $H = 1$, for $y = y_m$ and $\theta = \pi$: $-1 + \frac{au}{e(u)} \sin(2y_m) - \alpha_1 y_m = 1$ allows to compute y_m and α_1. This gives:

$$y_m = \frac{1}{2} g\left(\frac{e(u)}{2au}\right) \quad and \quad \alpha_1 = \frac{2au}{e(u)} \cos(2y_m)$$

where g is the inverse of the function $\sin x - x\cos x$ for $0 < x < \pi$.

References

[1] ARNOLD V.I. 1966 On an apriori estimate in the theory of hydrodynamic stability. *Izv. Vyssh. Uchebn. Zaved. Matematika* ***54*** (5) 3-5; Engl . transl.*: Am. Math. Soc. Trans.,* **79** *(2) 267-269* (1966).

[2] BARRE, J. BOUCHET, F. DAUXOIS, T. and RUFFO, S. 2002a Out-of-equilibrium states as statistical equilibria of an effective mean-field dynamics. *PRL* **89,** 11, 110601.

[3] BEEBE, R.F. and YOUNGBLOOD L.A. 1979 Pre-Voyager velocities, accelerations and shrinkage rates of Jovian cloud features, *Nature* **280**, 771-772.

[4] BOUCHET, F. 2001 Mécanique statistique pour des écoulements géophysiques. *PHD-Thesis Université Joseph Fourier-Grenoble.* available on *www.docs.unifi.it/~bouchet*

[5] BOUCHET, F. 2003 Parameterization of two dimensional turbulence using an anisotropic maximum entropy production principle. *Submitted to Physics of Fluids*

[6] BOUCHET F. and BARRE J. 2003 Classification of phase transitions and ensemble inequivalence, in systems with long range interactions. *submitted to J. Stat. Phys cond-mat 0303307*

[7] BOUCHET, F., CHAVANIS, P.H. and SOMMERIA, J. 2003 Statistical mechanics of Jupiter's Great Red Spot in the shallow water model. *preprint.*

[8] BOUCHET F. and SOMMERIA J. 2002 Emergence of intense jets and Jupiter's Great Red Spot as maximum entropy structures, *J. Fluid Mech.* **464** 165-207.

[9] BUSSE 1983 A model of mean zonal flows in the major planets *Geophys. Astrophys. Fluid Dyn.* **23**, 153-174.

[10] CHAVANIS, P.H. & SOMMERIA, J. 1996a Classification of self-organized vortices in two-dimensional turbulence: the case of a bounded domain. *J. Fluid Mech.* **134**, 267.

[11] CHAVANIS, P.H. SOMMERIA, J. and ROBERT, R. 1996b Statistical mechanics of two-dimensional vortices and collisionless stellar systems. *Astr. Jour.* **471**, 385-399.

[12] CHAVANIS, P.H. 1998 From Jupiter's great red spot to the structure of galaxies: statistical mechanics of two-dimensional vortices and stellar systems *Annals of the New York Academy of Sciences.* **867**, 120-141.

[13] CHAVANIS, P.H. and SOMMERIA J. 2002 Statistical mechanics of the shallow water system

[14] CHEN, P. & CROSS, M.C. 1996 Mean field equilibria of single coherent vortices *Phys. Rev. E* ***54,*** 6356-6363.

[15] DIBATTISTA, M.T. MAJDA, A.J. and GROTE, M. 2001 *Physica D*

[16] DOWLING, T.E 1995 Dynamics of Jovian Atmospheres, *Annu. Rev. Fluid Mech*, **27**, 293-334.

[17] DOWLING, T.E. and INGERSOLL, A.P. 1988 Potential vorticity and layer thickness variations in the flow around Jupiter's Great Red Spot and White Oval BC. *J.Atmos.Sci.* **45**, 1380-1396 .

[18] DOWLING, T.E. and INGERSOLL, A.P. 1989 Jupiter's Great Red Spot as a Shallow Water System *J.Atmos.Sci.* **46**, 3256-3278 .

[19] ELLIS, R.S., HAVEN K. and TURKINGTON, B. 2000 The Large Deviation Principle for Coarse-Grained Processes*, Physica A*

[20] ELLIS, R.S., HAVEN K. and TURKINGTON, B. 2002 Nonequivalent Statistical Equilibrium Ensembles and Refined Stability Theorems for Most Probable Flows*, Nonlinearity* 15:239-255.

[21] HATZES, A. WENKERT, D.D. INGERSOLL, A.P. and DANIELSON, G.E 1981 Oscillations and Velocity Structure of a Long-Lived Cyclonic Spot. *J.Geop.Res.* **86**, (A10), 8745-8749.

[22] HOLM, D.D. MARSDEN, J.E. RATIU, T. and WEINSTEIN, A. 1985 Nonlinear stability of fluid and plasma equilibria, *Physics report* **123**, Nos 1 & 2 1-116

[23] INGERSOLL, A.P. DOWLING, T.E. GIERASCH, P.J. ORTON, G.S. READ, P.L. SANCHEZ-LAVEGA, A. SHOWMAN, A.P. SIMON-MILLER, A.A. and VASAVADA, A.R. Dynamics of Jupiter's Atmosphere, *in Jupiter: The planet, Satellites & Magnetosphere,* Bagenal, F. McKinnon, W. Dowling, T. editors.

[24] INGERSOLL, A.P. GIERASCH, P.J BANFIEL, D. and VASAVADA, A.R. and the Galileo Imaging Team. 2000 Moist convection as an energy source for the large-scale motions in Jupiter's atmosphere. *Nature* **403**, 630-632

[25] JOYCE, G. and MONTGOMERY, D. 1973 Negative temperature states for the two-dimensional guiding center plasma. *J. Plasma Phys* **10**, 107-121

[26] KIDA, S. 1981 Motion of an elliptic vortex in a uniform shear flow. *J. Phys. Soc. Japan.* **50**, 3517-3520.

[27] KAZANTZEV, E. SOMMERIA, J. and VERRON, J. 1998 Subgridscale Eddy Parameterization by Statistical Mechanics in a Barotropic Ocean Model. *J.Phys.Ocean.* **28** (6) 1017-1042.

[28] KUKHARKIN, N. and ORSZAG, S.A. 1996 Generation and structure of Rossby vortices in rotating fluids. *Phys. Rev. E.* **54** (5) 13 4524-4527.

[29] KUZ'MIN, G.A. 1982 Statistical mechanics of the organization into two-dimensional coherent structures. *in "Structural Turbulence"* (ed M. A. Golgshtik), pp 103-114. Acad. Naouk CCCP Novosibirsk, Institute of Thermophysics.

[30] LIMAYE, S.S. 1986. Jupiter : new estimates of the mean zonal flow at the cloud level *Icarus* **65** 335-52.

[31] MARCUS, P.S. 1993. Jupiter's Great Red Spot and other vortices. *Annu. Rev. Astron. Astrophys.* **31** 523-73.

[32] MAXWORTHY, T. 1984. The dynamics of a high-speed Jovian jet. *Planet. Space Sci.* **32** 8. 1053-1058.

[33] MAXWORTHY, T. and REDEKOPP L. 1976. A solitary wave theory of the Great Red Spot and other observed features in the Jovian atmosphere *Icarus* **29** 261-271. MEYERS S.D., SOMMERIA J. and SWINNEY H.L. (1989) " Laboratory study of the dynamics of Jovian-type vortices", *Physica D* **37** 515-530.

[34] MICHEL, J. and ROBERT, R. 1994a Statistical mechanical theory of the great red spot of Jupiter. *J. Phys. Stat.* **77** (3/4), 645-666.

[35] MICHEL, J. and ROBERT, R. 1994b Large Deviations for Young measures and statistical mechanics of infinite dimensional dynamical systems with conservation law. *Commun. Math. Phys.* **159**, 195-215.

[36] MILLER, J. 1990 Statistical mechanics of Euler's equation in two dimensions. *Phys. Rev. Lett.* **65** (17), 2137.

[37] MILLER, J. WEICHMAN, P.B. and CROSS, M.C. 1992 Statistical mechanics, Euler's equation, and Jupiter's Red Spot. *Phys. Rev. A.* ***45*** (4), 2328-2359.

[38] MITCHELL, J.L. BEEBE, R.F. INGERSOLL, A.P. and GARNEAU, G.W. 1981 Flow fields within Jupiter's Great Red Spot and White Oval BC. *J. Geophys.Res.* **86**, 8751-8757.

[39] MODICA, L. 1987 Gradient theory of phase transitions and minimal interface criteria. *Arch. Rational. Mech. Anal.* **98** 123-142.

[40] MORALES-JUBERIAS, R. SANCHEZ-LAVEGA, A. LECACHEUX, J. and COLAS, F. 2002 A comparative study of jovian anticyclone properties from a six year (1994-2000) survey. *Icarus* **157**, 76-90

[41] ONSAGER, L. 1949 Statistical hydrodynamics. *Nuovo Cimento Suppl.* **6** (3), 279.

[42] POLVANI, L.M. WISDOM, J. DELONG, E. and INGERSOLL, A.P. 1990 Simple Dynamic-Models of Neptune Great Dark Spot. *Science* **249**, 1393-1398

[43] PEDLOSKY, J. 1987 Geophysical Fluid Dynamics, Second Edition. *Springer Verlag*

[44] PETVIASHVILI V. I., 1981, Red Spot of Jupiter and the drift soliton in a plasma, JETP Lett. 32(11), 619-622.

[45] READ, P.L. and HIDE R. 1984. An isolated baroclinic eddy as a laboratory analogue of the Great Red Spot on Jupiter, *Nature* **308**, 45-48.

[46] RHINES, P.B. and YOUNG, W.R. 1982. Homogenization of potential vorticity in planetary gyres. **122**, 347-367

[47] ROBERT, R. 1990 Etat d'équilibre statistique pour l'écoulement bidimensionnel d'un fluide parfait. *C. R. Acad. Sci. Paris* **311** (I), 575-578.

[48] ROBERT, R. 2000 On the statistical mechanics of 2D Euler and 3D Vlasov Poisson equations, *Comm. Math. Phys.* **212**, 245-256.

[49] ROBERT, R. and SOMMERIA, J. 1991 Statistical equilibrium states for two-dimensional flows, *J. Fluid. Mech.* **229**, 291-310

[50] ROBERT, R. and SOMMERIA, J. 1992 Relaxation towards a statistical equilibrium state in two-dimensional perfect fluid dynamics, *Phys. Rev. Lett.* **69**, 2776-2779

[51] ROBERT, R. and ROSIER, C. 1997 The modeling of small scales in 2D turbulent flows: a statistical mechanics approach. *J. Stat. Phys.* **86**, 481-515

[52] SALMON, R. 1988 Hamiltonian fluid mechanics. *Ann. Rev. Fluid Mech.* **20**, 225-256

[53] SANCHEZ-LAVEGA and collaborators, 2001 The merger of two giant anticyclones in the atmosphere of Jupiter. *Icarus* **149,** 491-495

[54] SHEPHERD, T. G. 1990 Symmetries, conservation laws, and Hamiltonian structure in geophysical fluid dynamics. *Adv. Geophys.* **32,** 287-338

[55] SOMMERIA, J. 2001 Two-dimensional turbulence, in "New trends in turbulence" (Les Houches 2000), edited by M. Lesieur, A. Yaglom et F.David, EDP/Springer.

[56] SOMMERIA, J. NORE, C. DUMONT,T and ROBERT, R. 1991 Théorie statistique de la Tache Rouge de Jupiter. *C.R. Acad. Sci* **t. 312**, Série II p 999-1005.

[57] SOMMERIA, J. STAQUET, C. and ROBERT, R. 1991 Final equilibrium state of a two dimensional shear layer *J.Fluid Mech.* **233**, 661.

[58] TURKINGTON, B MAJDA, A. HAVEN, K. and DIBATTISTA, M. 2001 Statistical equilibrium predictions of jets and spots on Jupiter *PNAS,* **98,** 22, 12346-12350

[59] TURKINGTON, B. and WHITAKER, N. 1996 Statistical equilibrium computations of coherent structures in turbulent shear layers *SIAM J. Sci. Comput.* **17** (16), 1414.

[60] YANO, J. TALAGRAND, O. and DROSSART, P. 2002 Multiple jets in the atmosphere of the Giant outer planets simulated by an idealized deep-fluid model.

[61] YONGMING, L. MU, M. and SHEPERD, T.G. 1996 Nonlinear stability of continuously stratified quasi-geostrophic flow. *J. Fluid. Mech.,* **325,** 419-469

Figure Captions.

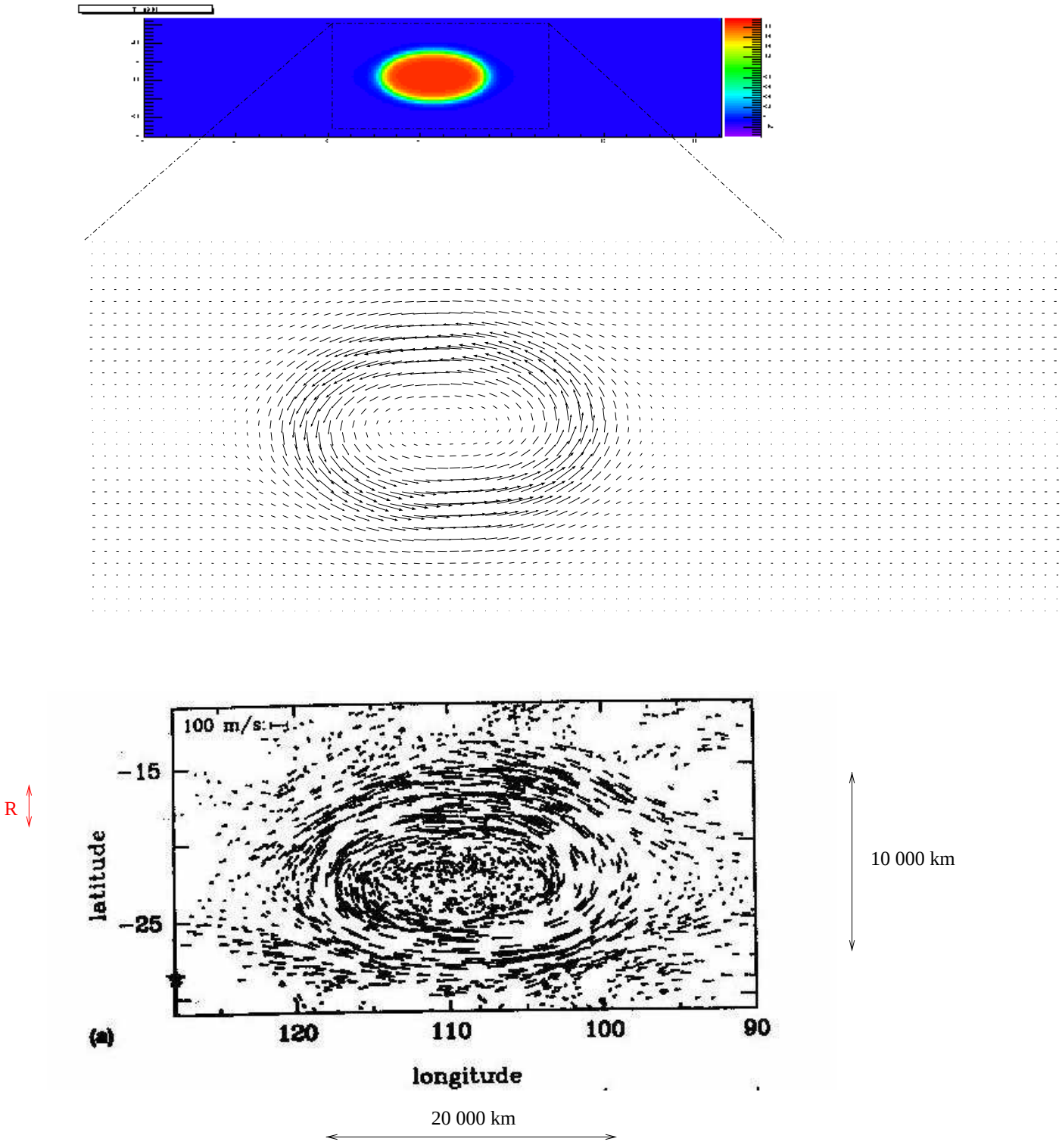

Figure 1: Upper part: vorticity field and velocity field for the statistical equilibrium modeling the Great Red Spot. Lower : the observed velocity field, from Dowling and Ingersoll (1988). The actual values of the jet maximum velocity, jet width, vortex width and length fit with the observed ones. The strong jet is the interface between two phases, each corresponding to different Potential Vorticity mixing. It obeys a minimal length variational problem, balanced by the effect of the deep layer shear.

Figure 2: The area free energy $f_C(\phi)$ specifying the free energy functional (16). For any value of C , the function $f_C(\phi)$ is even and possess two minima $\pm u$. This shows that, at equilibrium, at zeroth order in R, the Potential Vorticity mixing will be described by two phases, characterized by these two minima. This plot corresponds to the value $C = 10$.

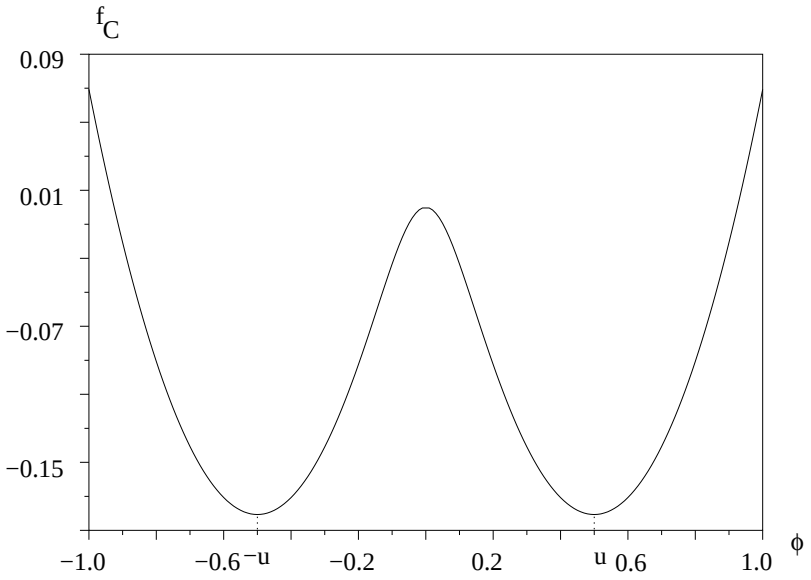

Figure 3: At zeroth order, ϕ takes the two values $\pm u$ on two subdomains $A_{\pm}$. These subdomains are separated by strong jets. The actual shape of the structure, or equivalently the position of the jets, is given by the first order analysis.

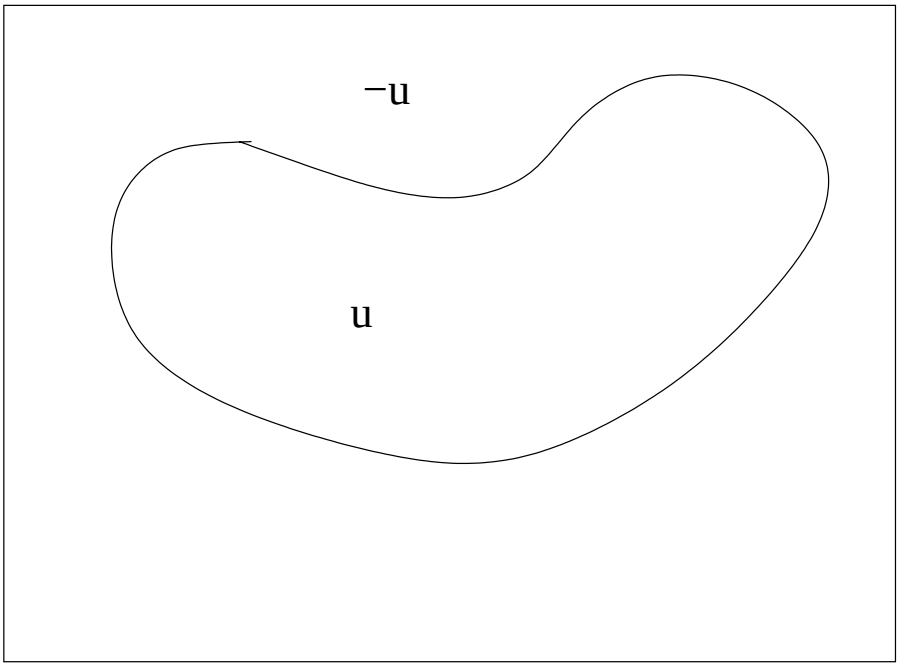

Figure 4: Phase diagram of the Gibbs states versus the energy E and the asymmetry parameter B (see (9)), when no topography is present ($h = 0$). The outer solid line is the maximum energy achievable for a fixed B : $E = \frac{R^2}{2}(1 - B^2) + \mathcal{O}\left(R^3\right)$. Straight jets are obtained for the nearly symmetric cases (B around 0), while a vortex is formed when one of the PV levels has a lower area. This vortex takes the form of a circular jet for sufficiently high energy. The frontiers line between the straight jets and the circular jet is determined by the minimization of the jet length (first order free energy). The hashed line represents the energy value for which vortex area A_1 or A_{-1} (21) is equal to $(2l)^2$, where l is the typical jets width. At the left of this line, the small Rossby deformation radius asymptotic expansion is no more valid. For such case, asymmetric equilibrium have been described in Bouchet and Sommeria (2002). This hashed line depends on the value of R, the ratio of the Rossby deformation radius to the domain scale. It has been here numerically calculated for R = 0.03.

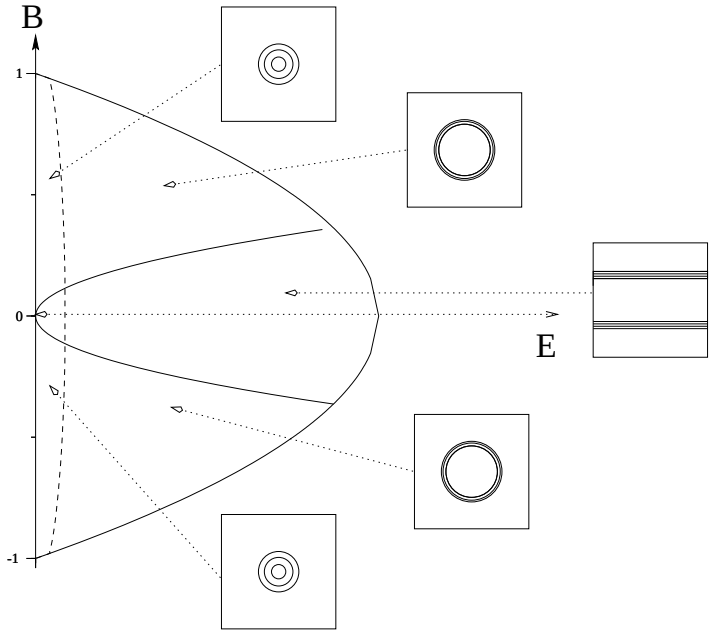

newpage

Figure 5: Top: typical vortex shape obtained from the curvature radius equation (26) for two values of the parameters (arbitrary units). This illustrate the very characteristic particularity of Jupiter's vortices to be vary elongated, ones they reach an extremal latitude y_m (27). Bottom left: the Great Red Spot and one of the White Ovals. Bottom right: one of the Brown Barges of Jupiter's north atmosphere. This shows that equilibrium structures are able to reproduce the characteristic and peculiar elongation of jovian vortices.

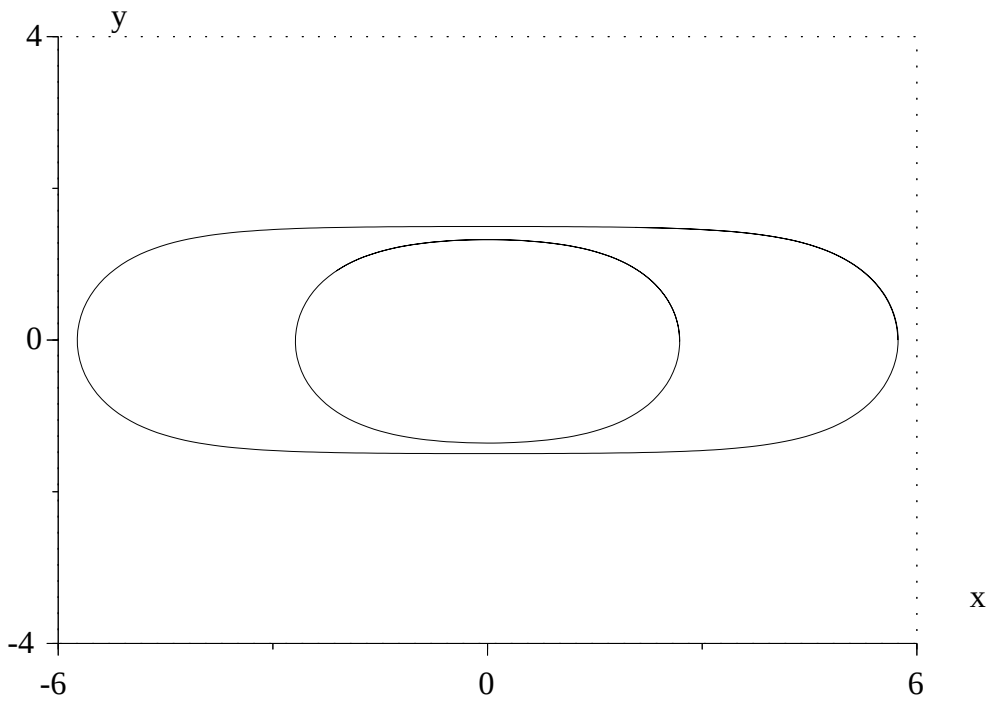

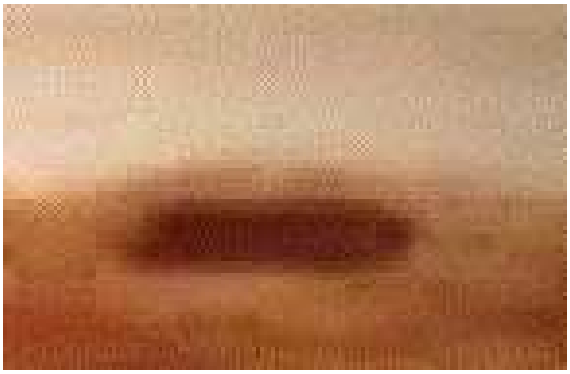

Figure 6: QG topography (units s^{-1}) versus latitude computed using the data of Dowling and Ingersoll (1989) : a) under the GRS ; b) under the Oval BC. The analysis of the velocity data in the Quasi-Geostrophic framework, thus clearly shows extrema of topography under these two vortices. This is in accordance with what we deduce from the statistical equilibrium study.

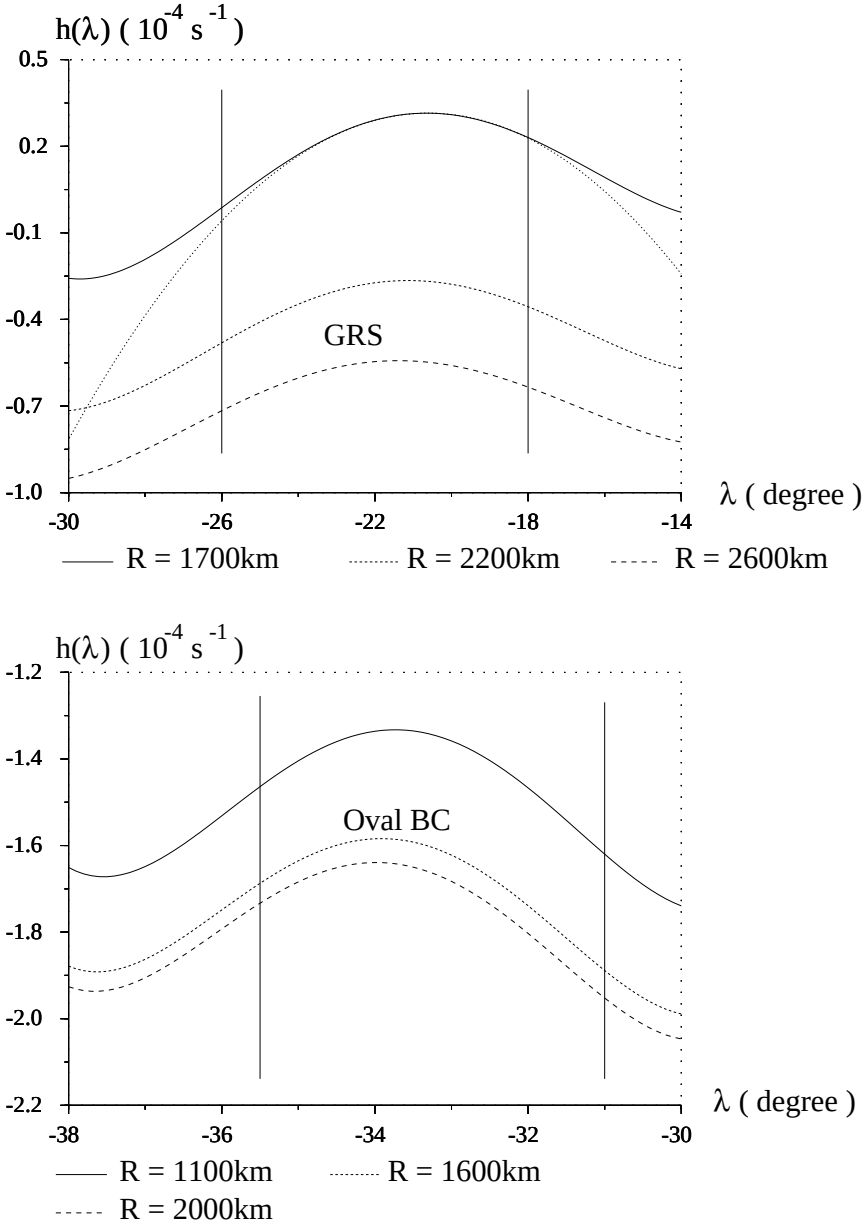

Figure 7: Phase diagram of the Gibbs states versus the energy E and the asymmetry parameter B, with a quadratic topography and a domain aspect ratio corresponding to the Great Red Spot parameters. (400.000 km over 20.000 km). The outer line is the maximum energy achievable for a fixed B : $E = \frac{R^2}{2}(1-B^2)+\mathcal{O}\left(R^3\right)$. The inner solid line corresponds to the frontier between the vortex and straight jet solutions. The dash line corresponds to the limit of validity of the small deformation radius hypothesis. It has been drawn using the condition that the maximal vortex width (28) is equal to two Rossby deformation radius. The dot lines are constant vortex aspect ratio lines with values 2,10,20,30,40,50,70,80 respectively. We have represented only solutions for which anticyclonic PV dominate ($B > 0$). The opposite situation may be recovered by symmetry.

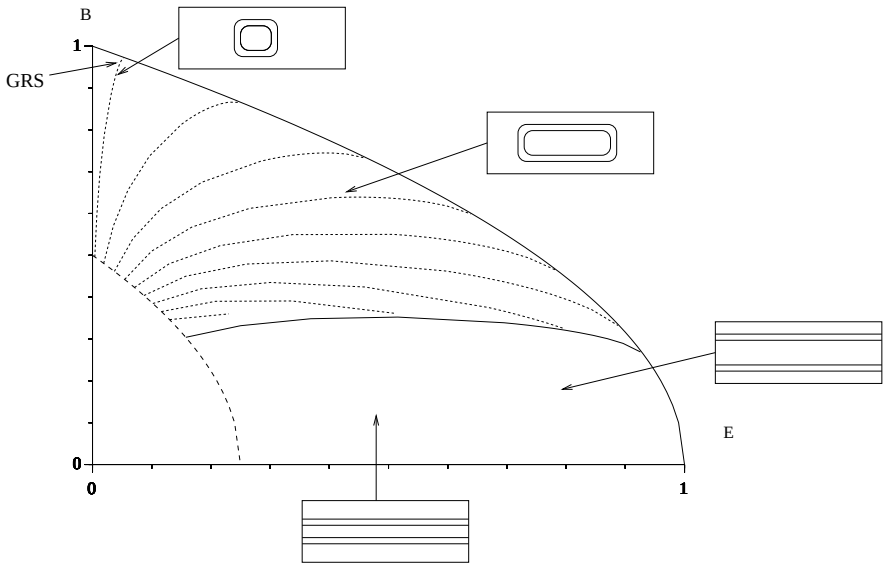

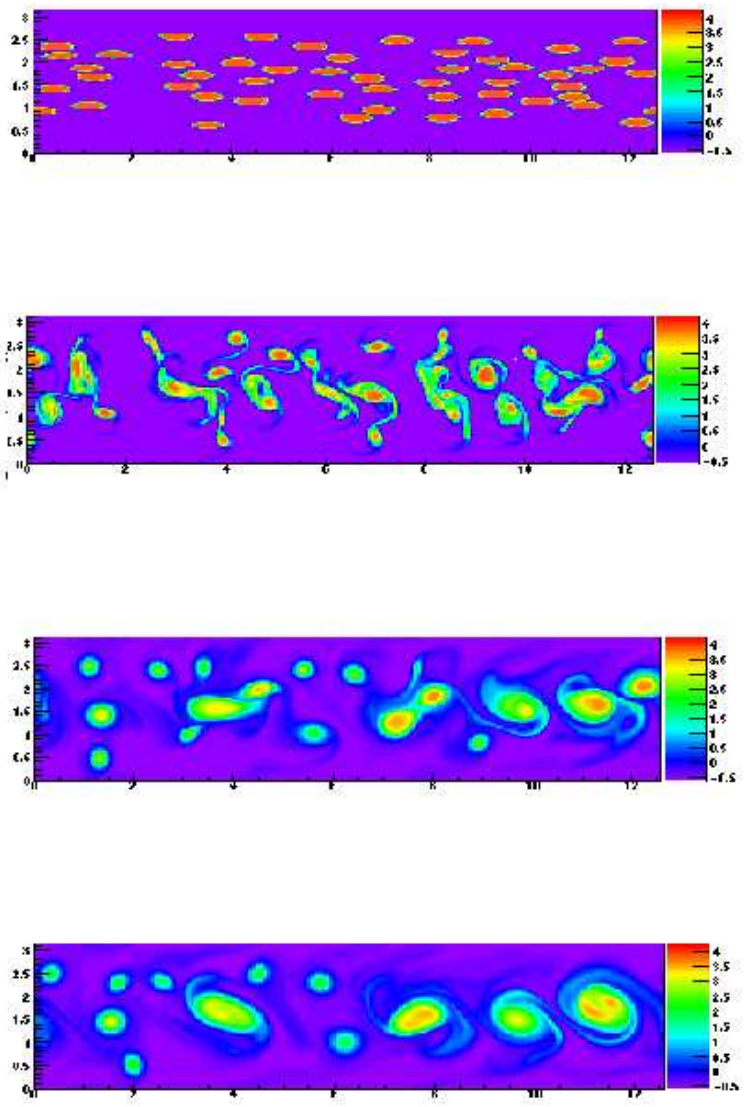

Figure 8: Dynamics of random initial vorticity patches, in the Quasi-Geostrophic model, using a small scale parameterization based on a maximum entropy production principle (29). The color represents the PV values. The Rossby deformation radius is very small ($R = 0.2$), compared to the latitudinal band width (π). We use a cosine topography (4) whose maxima is located at the center of the latitudinal band. The later evolution is shown on figures 9 and 10

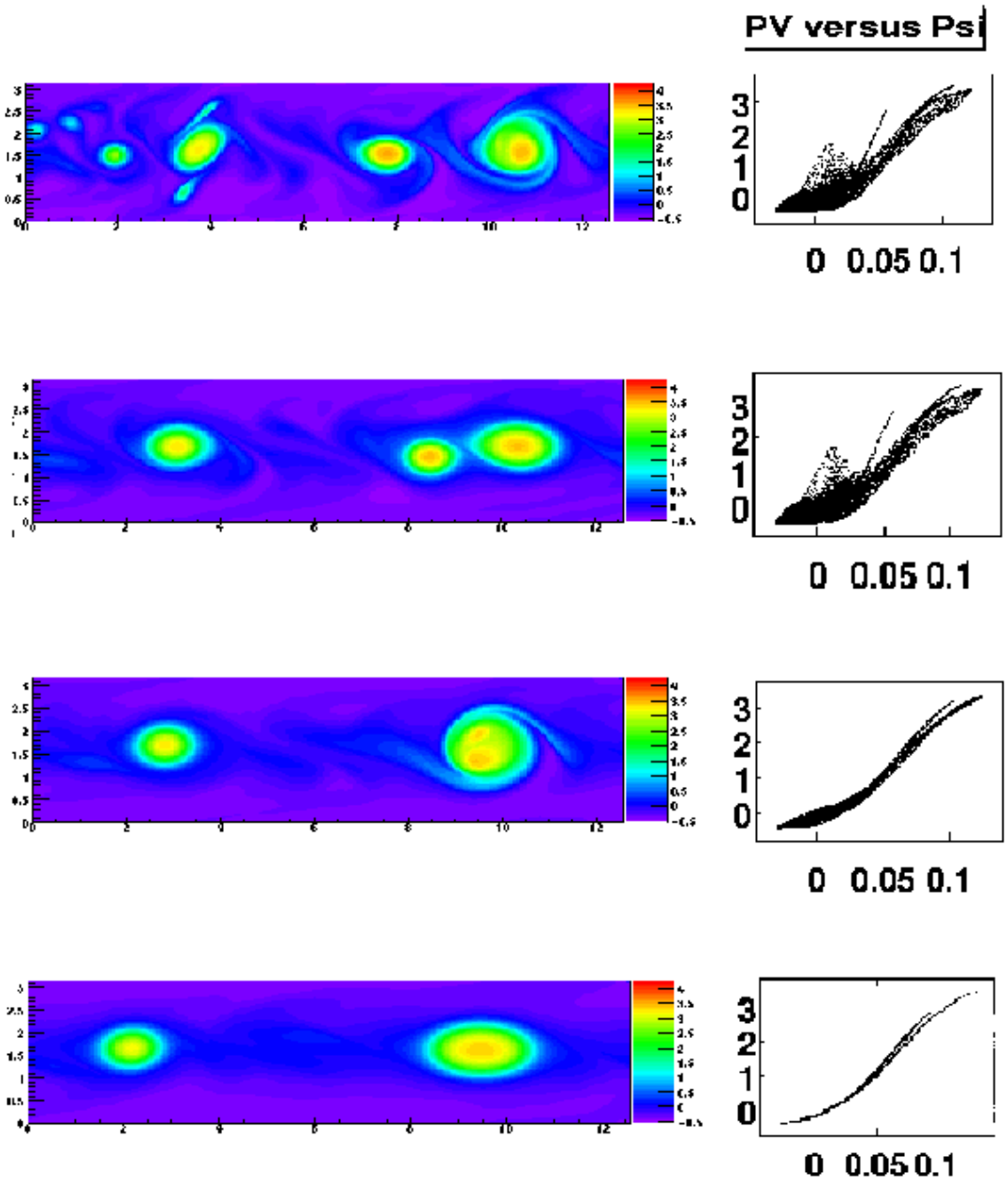

Figure 9: Continuation of the previous figure. After a very rapid local organization, three anticyclones form. On a much longer time scale, they merge, forming elongated vortices similar to the White Ovals on the jovian troposphere (the time lapse between the scatter-plots of figure 8 is approximately 16 turn over times, whereas between the two last scatter plots of this figure it is 50 turn over times, and 300 to obtain the final organization represented on figure 10. The insets show Stream function-PV scatter plots. They illustrate the evolution towards stationary states.

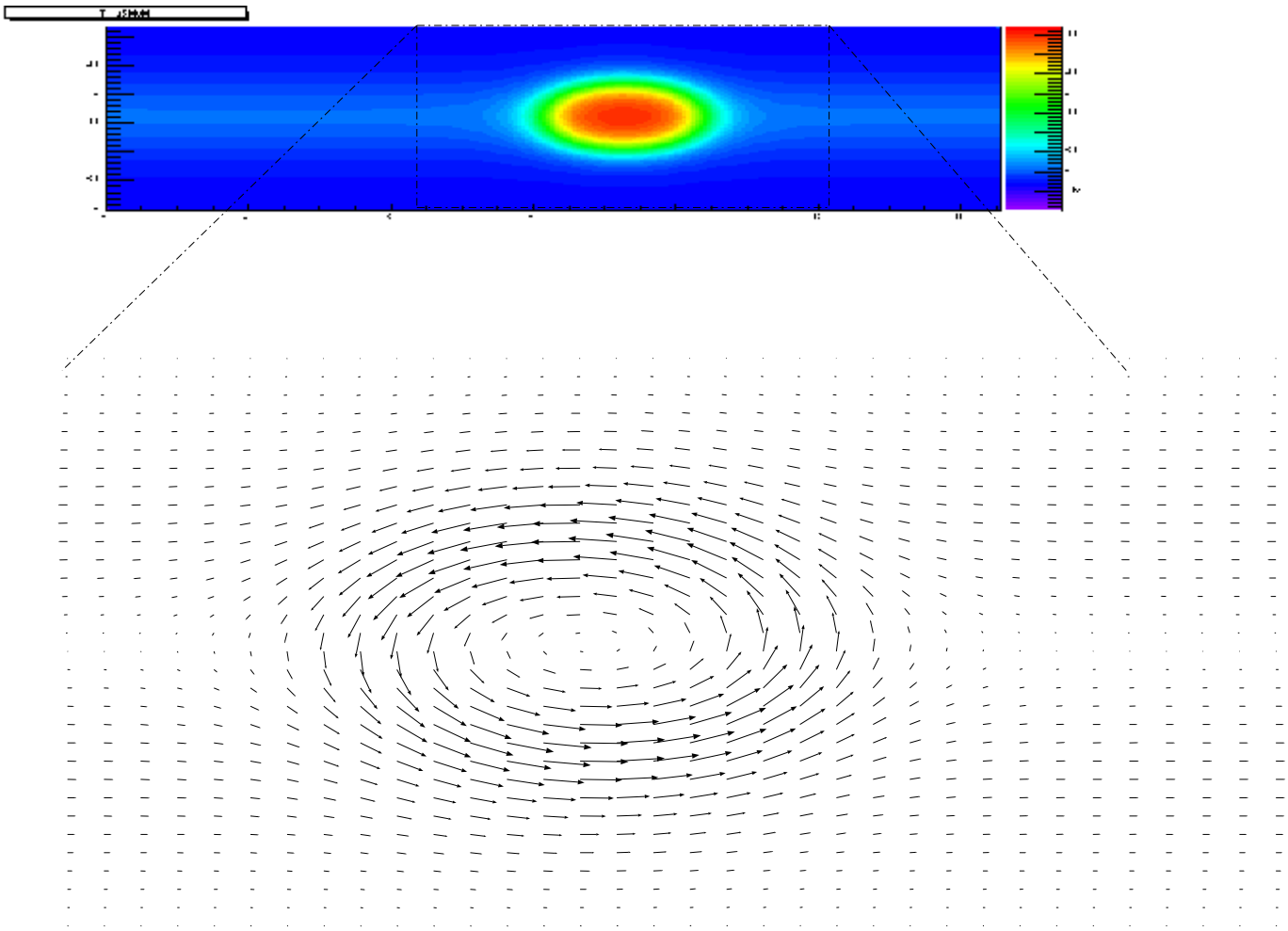

Figure 10: Equilibrium structures corresponding to the dynamical evolution of the two preceding figures. The upper figure is the PV, whereas the lower one is the velocity field. The maxima of entropy under constraint is an anticyclone, centered on the maxima of the topography. The surrounding shears and its oval shape are consequences of its interaction with the deep layer flow (topography). This structure is similar to the one of the White Ovals. It differs from the Great Red Spot, because the Rossby deformation radius is of the same order as the vortex size.

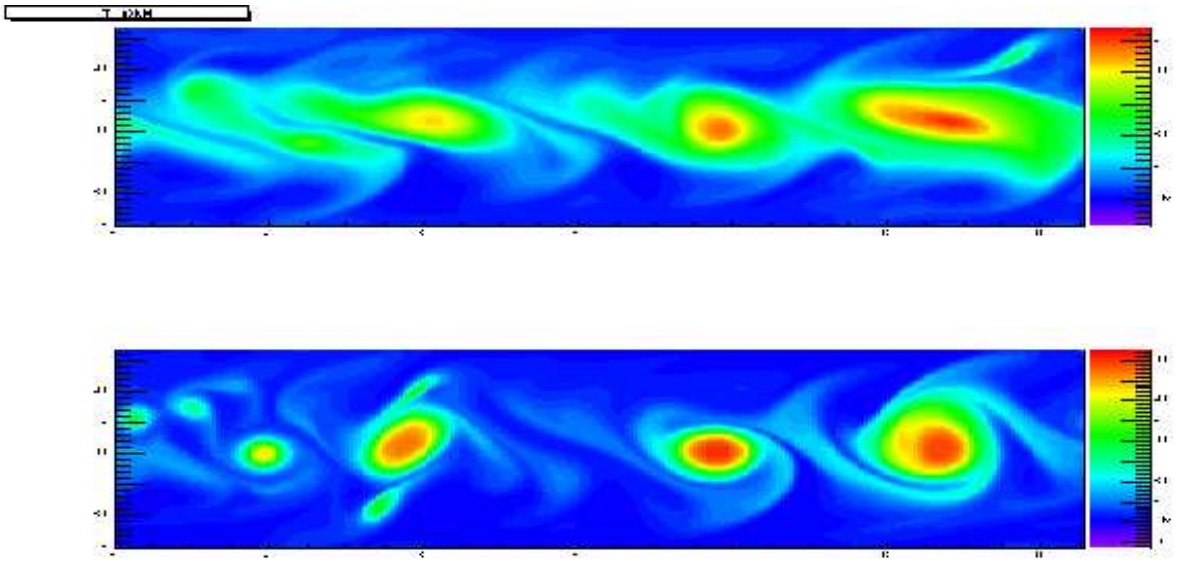

Figure 11: Comparison of the evolution of the same initial condition, made of random vorticity patches (the same as for the three previous figures), for two different small scale Potential Vorticity mixing parameterization. The upper figure shows the result for a Direct Numerical Simulation (usual eddy diffusivity), the upper one shows the results for the relaxation equations (29). This shows that the Direct Numerical Simulation does not allowed to obtain strong coherent vortices, for very long times.

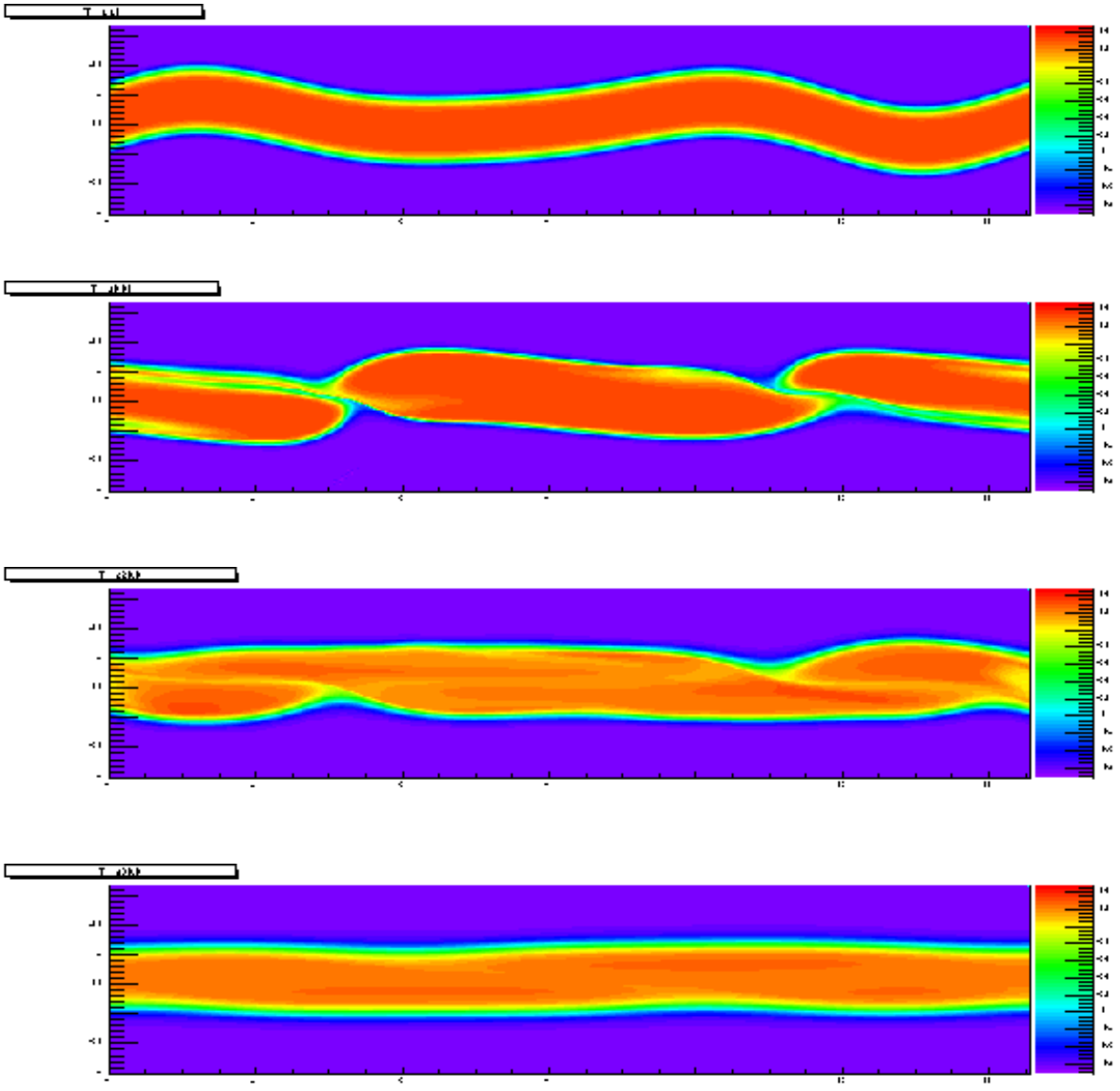

Figure 12: Potential Vorticity field, for two jets flowing eastward and westward respectively. Whereas they do not verify the two Arnold's theorem hypothesis, submitted to a strong perturbation, they stabilize. The maximization of the entropy under constraint allow to obtain new stability theorems (see section 5).

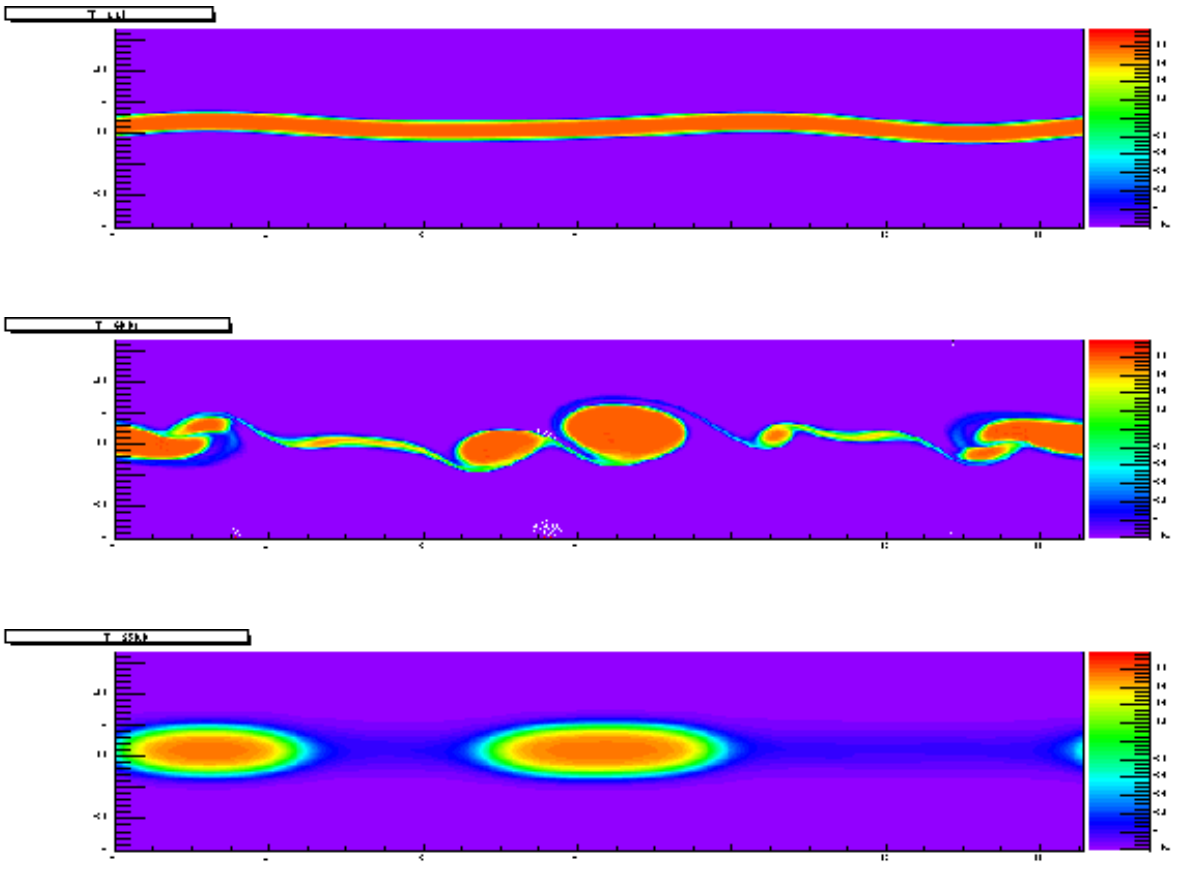

Figure 13: Destabilization of two strong jets, and formation of very elongated vortices similar to the cyclonic Brown Barges in the north hemisphere of the Jovian atmosphere. The stability property of such jets and vortices is summarized by the phase diagram on figure 7 (see section 5).

Figure 14: The upper figure shows the Potential Vorticity field for a statistical equilibrium on a strong topography. The shape of the spot can be compared to real image of the Brown Barges (figure 5). The four lower figures show the velocity for a zonal section (eastward velocity, left figures) and for a meridional section (northward velocity, right figures). The two upper velocity figures are the observed ones for one of the cyclonic Brown Barges, in the north hemisphere of Jupiter (from Hatzes and collaborators (1981)). The two lower ones are the statistical equilibrium ones.